Society for
Mathematical
Biology

Check for
updates

Investigating the Influence of Growth Arrest Mechanisms on Tumour Responses to Radiotherapy

Chloé Colson[1] [ID] · **Philip K. Maini[1]** · **Helen M. Byrne[1,2]**

Abstract

Cancer is a heterogeneous disease and tumours of the same type can differ greatly at the genetic and phenotypic levels. Understanding how these differences impact sensitivity to treatment is an essential step towards patient-specific treatment design. In this paper, we investigate how two different mechanisms for growth control may affect tumour cell responses to fractionated radiotherapy (RT) by extending an existing ordinary differential equation model of tumour growth. In the absence of treatment, this model distinguishes between growth arrest due to nutrient insufficiency and competition for space and exhibits three growth regimes: nutrient limited, space limited (SL) and bistable (BS), where both mechanisms for growth arrest coexist. We study the effect of RT for tumours in each regime, finding that tumours in the SL regime typically respond best to RT, while tumours in the BS regime typically respond worst to RT. For tumours in each regime, we also identify the biological processes that may explain positive and negative treatment outcomes and the dosing regimen which maximises the reduction in tumour burden.

Keywords Fractionated radiotherapy · Heterogeneity · Growth-limiting mechanisms · Ordinary differential equations

---

Philip K. Maini and Helen M. Byrne authors contributed equally to this work.

✉ Chloé Colson
chloe.colson@maths.ox.ac.uk

Philip K. Maini
philip.maini@maths.ox.ac.uk

Helen M. Byrne
helen.byrne@maths.ox.ac.uk

[1] Wolfson Centre for Mathematical Biology, Mathematical Institute, University of Oxford, Radcliffe Observatory Quarter, Oxford OX2 6GG, UK

[2] Ludwig Institute for Cancer Research, Nuffield Department of Medicine, University of Oxford, Roosevelt Drive, Oxford OX3 7DQ, UK

🙋 Springer

1 Introduction

Understanding the biological mechanisms underpinning cancer and developing effective therapeutic protocols to improve patient prognosis are fundamental aims of cancer research. Existing treatment modalities, such as radiotherapy (RT) and chemotherapy (CT), are applied via highly-regulated dosing protocols (National Cancer Institute 2019, 2022) to avoid damaging healthy tissue, while maximising treatment effect. Nonetheless, the efficacy of both RT and CT is limited by their intolerable side-effects. Further, inter-tumour heterogeneity can significantly influence sensitivity to treatment. Investigating how different growth mechanisms may affect response to treatment is, therefore, an important step towards overcoming barriers to treatment efficacy. In this paper, we investigate how two distinct growth-rate limiting mechanisms, namely growth arrest in response to nutrient insufficiency and to competition for space, impact tumour response to RT.

A dynamic model of tumour growth that distinguishes between mechanisms of tumour control. Regardless of their biological complexity, existing models of solid tumour growth typically describe a single mechanism by which a tumour may reach an equilibrium. For example, the models developed by Enderling et al. (2006), Hahnfeldt et al. (1999), Liu et al. (2021), Milzman et al. (2021) and Zahid et al. (2021) predict growth arrest due to a cessation of proliferation (with no explicit cell death), while those proposed by Drasdo and Höhme (2005), Greenspan (1972), Hillen et al. (2013) and Lewin et al. (2020) predict growth arrest due to the balance of cell proliferation and cell death.

In previous work (Colson et al. 2022), we developed a model of solid tumour growth that simultaneously describes growth arrest due to nutrient inhibition, when the net rates of cell proliferation and death are equal (and strictly positive), and growth arrest due to contact inhibition, when the net rate of cell proliferation becomes zero, with no cell death. We assumed that the system is well-mixed and neglected angiogenesis and vascular remodelling. In particular, we viewed the vascular volume as a parameter which influences nutrient and space availability and, therefore, the tumour's carrying capacity. As such, the model does not capture the co-evolution of the vasculature with tumour cells that is observed *in vivo* and that can allow nutrient limited tumours to continue to grow (see Discussion). Nor does it describe how secondary tumours are established, i.e., metastasis.

The model comprises two time-dependent ordinary differential equations (ODEs) for the tumour volume, $T(t)$, and the oxygen concentration, $c(t)$, and can be written as follows:

$$\frac{\mathrm{d}T}{\mathrm{d}t} = \underbrace{q_2^* c T (S_{max} - (T + V_0))}_{\substack{\text{rate of} \\ \text{tumour cell proliferation}}} - \underbrace{\left[\delta_1^*(c_{min}^* - c)\right] H(c_{min}^* - c)T}_{\substack{\text{rate of} \\ \text{cell death due to nutrient starvation}}} \quad , \tag{1}$$

$$\frac{\mathrm{d}c}{\mathrm{d}t} = \underbrace{g^*(c_{max}^* - c)V_0}_{\substack{\text{rate of} \\ \text{nutrient delivery}}} - \underbrace{q_1^* c T}_{\substack{\text{baseline rate of} \\ \text{nutrient consumption}}} - \underbrace{q_3^* c T (S_{max} - (T + V_0))}_{\substack{\text{additional rate of} \\ \text{nutrient consumption for proliferation}}} \tag{2}$$

where

$$H(x) = \begin{cases} 1, & \text{if } x \geq 0, \\ 0, & \text{if } x < 0. \end{cases} \tag{3}$$

Denoting the total available space by S_{max} (m^3) and the vascular volume by V_0 (m^3), the rate of tumour cell proliferation is assumed to be proportional to the available free space, $S_{max} - T - V_0$, and to the oxygen concentration, c, with proportionality constant q_2^* $(\text{kg}^{-1}\text{min}^{-1})$. If c drops below a threshold value, c_{min}^* (kg m^{-3}), then cells die at a rate proportional to the difference between c and c_{min}^*, with proportionality constant δ_1^* $(\text{m}^3\text{kg}^{-1}\text{min}^{-1})$. Further, oxygen is supplied to the tumour at a rate proportional to V_0 and the difference between the oxygen concentration in the vasculature, c_{max}^* (kg m^{-3}), and in the tumour. The parameter g^* $(\text{m}^{-3}\text{min}^{-1})$ is the rate of oxygen exchange per unit volume area of blood vessel. Finally, oxygen is consumed by tumour cells for maintenance at a rate proportional to c, with rate constant q_1^* $(\text{m}^{-3}\text{min}^{-1})$, and for proliferation at a rate proportional to the proliferation rate, with conversion factor $k > 0$ defined such that $q_3^* = q_2^*/k$ $(\text{m}^{-6}\text{min}^{-1})$.

Since the model (1), (2) distinguishes between two mechanisms for growth-control, it can be used to investigate how they impact tumour response to treatment. Therefore, in this work, we extend Eqs. (1), (2) to account for the biological effects of RT.

Radiobiology. RT is used to treat more than 50% of cancer patients (Maier et al. 2016). It involves the delivery of energy rays, via small doses called fractions, at regular time intervals and over a fixed period of time, to a region of the body comprising both cancerous and healthy tissue. Radiation protocols are, therefore, designed to balance treatment efficacy and undesirable side-effects in normal tissues. While a conventional fractionation schedule consists of 2 Gy doses delivered Monday to Friday for up to 7 weeks (Ahmed et al. 2014), the dose, dosing frequency and treatment duration can be varied to deliver a fixed total dose. The latter is often termed the Maximum Tolerated Dose, i.e., the highest dose which does not cause adverse side-effects (Gad 2014).

Radiation induces direct and indirect cytotoxic effects by causing DNA damage to cancer cells that is fatal if left unrepaired. Direct effects arise from interactions between ionising particles and DNA and indirect ones from interactions between ionising particles and water, which create reactive oxygen species that subsequently react with DNA. Indirect effects are the most common, which is why hypoxic, i.e., poorly oxygenated, tumours are often radio-resistant (Graham and Unger 2018). Intratumoural oxygen levels are a key factor influencing tumour radio-sensitivity, and another key factor are tumour cell proliferation rates, as cells that are in the G2 or mitosis phases of the cell cycle are the most sensitive to RT.

RT can also affect the tumour vasculature, with increases in angiogenesis observed at low doses (Marques et al. 2020) and vascular damage and necrosis observed at high doses (Stolz et al. 2022; Venkatesulu et al. 2018). In this work, we neglect the effect of RT on vasculature in order to focus on evaluating how nutrient- and contact-inhibited growth control affect the sensitivity of tumour cells to treatment with RT.

Mathematical modelling of tumour response to radiotherapy. A number of mathematical models have been proposed to describe tumour response to RT. Key aims

of these modelling efforts include studying specific RT protocols (Enderling et al. 2010; Jeong et al. 2017; Lewin et al. 2018; Prokopiou et al. 2015; Rockne et al. 2009), designing patient-specific RT dosing schedules (Alfonso et al. 2014; Belfatto et al. 2018) and investigating the influence of inter- and/or intra- tumour heterogeneity on tumour sensitivity to RT (Alfonso and Berk 2019; Celora et al. 2023; Powathil et al. 2012; Enderling et al. 2009; Watanabe et al. 2016).

While the purpose of these modelling approaches may differ, they are all based on the common assumption that RT inflicts instantaneous cell death on tumour cells and the cell kill is modelled using the Linear-Quadratic (LQ) model (McMahon 2018). The LQ model states that the fraction, S_{LQ}, of (tumour) cells that survive exposure to a dose D (Gy) of radiation is given by

$$S_{LQ}(D) = \exp\left(-\left(\alpha D + \beta D^2\right)\right), \tag{4}$$

where $\alpha \geq 0$ and $\beta \geq 0$ are tissue-specific radio-sensitivity parameters. These parameters are typically derived from cell survival data collected at a small number of time points in *in vitro* two-dimensional (2D) monolayer or three-dimensional (3D) spheroid experiments. As such, they provide information about the long-term proportion of cell death rather than how the cell death rate changes over time. In contrast, a time-dependent description of RT cell kill can account for different types of damage (direct vs. indirect), damage repair and cell death following insufficient repair (Curtis 1986; Goodhead 1985; Neira et al. 2020; Tobias 1985). Such a description facilitates the study of the evolution of tumour composition during treatment, as we may keep track of changes in healthy, damaged and dead tumour cell populations. In this paper, we follow Neira et al. (2020) and adopt a time-dependent description of RT.

Paper structure. This paper is structured as follows. In Sect. 2, we extend the tumour growth model defined by Eqs. (1), (2) to account for the biological effects of RT. We summarise the key features of the model dynamics in the absence of treatment in Sect. 3. Then, we investigate the response of tumours characterised by different growth-limiting mechanisms in Sect. 4, initially performing a numerical study of tumour response during RT and, subsequently, looking at post-treatment growth dynamics via a steady state analysis and complementary numerical study. The paper concludes in Sect. 5, where we discuss our findings and outline possible avenues for future work.

2 Model Development

2.1 The Mathematical Model

In this section, we incorporate tumour response to RT into the growth model (1), (2). We follow the approach outlined in Neira et al. (2020) and adopt a time-dependent description of radiotherapy. In more detail, we introduce the dependent variables T_S and T_R to denote tumour cells that have been, respectively, sub-lethally and lethally damaged by RT. We suppose that the tumour is exposed to a total dose D (Gy) of RT

at a constant rate R over the time period $t_R \leq t \leq t_R + \delta_R$ (min) so that

$$R(t) = \begin{cases} D/\delta_R, & \text{if } t_R \leq t \leq t_R + \delta_R, \\ 0, & \text{otherwise.} \end{cases} \tag{5}$$

Let $\Sigma = T + T_S + T_R + V_0$ be the total tumour volume. We propose the following system of time-dependent ODEs to describe tumour growth and response to RT (see also the schematic in Fig. 1):

$$\frac{dT}{dt} = q_2^* c T (S_{max} - \Sigma) - \delta_1^* (c_{min}^* - c) H (c_{min}^* - c) T$$
$$- \underbrace{\lambda^* c R T}_{\substack{\text{rate of direct} \\ \text{lethal damage}}} - \underbrace{\nu^* c R T}_{\substack{\text{rate of} \\ \text{sub-lethal damage}}} + \underbrace{\mu^* T_S}_{\substack{\text{rate of} \\ \text{repair}}}, \tag{6}$$

$$\frac{dT_S}{dt} = q_{2,S}^* c T_S (S_{max} - \Sigma) - \delta_{1,S}^* (c_{min}^* - c) H (c_{min}^* - c) T_S$$
$$+ \nu^* c R T - \mu^* T_S - \underbrace{\xi^* T_S}_{\substack{\text{rate of} \\ \text{post-RT death} \\ \text{due to MC}}} - \underbrace{\lambda_S^* c R T_S}_{\substack{\text{rate of indirect} \\ \text{lethal damage}}}, \tag{7}$$

$$\frac{dT_R}{dt} = \lambda^* c R T + (\xi^* + \lambda_S^* c R) T_S - \underbrace{\eta_R^* T_R}_{\substack{\text{rate of} \\ \text{clearance}}}, \tag{8}$$

$$\frac{dc}{dt} = g^* (c_{max}^* - c) V_0 - q_1^* c T - q_3^* c T (S_{max} - \Sigma) - q_{1,S}^* c T_S - q_{3,S}^* c T_S (S_{max} - \Sigma), \tag{9}$$

where H is the Heaviside function defined in (3).

We assume that undamaged tumour cells, T, proliferate, die due to nutrient insufficiency and consume oxygen for proliferation and maintenance as in Eqs. (1), (2). They suffer sub-lethal and lethal damage during irradiation at rates proportional to the oxygen concentration, c, and the RT dose rate, R, with proportionality constants $\nu^* > 0$ and $\lambda^* > 0$, respectively. We further suppose that sub-lethal damage is either repaired at a constant rate $\mu^* > 0$, or leads to tumour cell death via two distinct pathways. First, sub-lethal damage may become lethal as it accumulates at a rate proportional to the oxygen concentration, c, and the RT dose rate, R, with proportionality constant $\lambda_S^* > 0$. Second, sub-lethally damaged cells, T_S, may also undergo mitotic catastrophe (MC) if they attempt to divide with mis- or un-repaired DNA damage; we assume this occurs at a constant rate $\xi^* > 0$.

Sub-lethally damaged cells, T_S, also consume oxygen for maintenance and proliferation, proliferate and die due to nutrient insufficiency similarly to undamaged cells, T, although at different rates. More specifically, they proliferate at a rate proportional to the oxygen concentration, c, and the available space, with proportionality constant $q_{2,S}^* = \theta_2 q_2^* > 0$, with $\theta_2 \in (0, 1)$. The latter ensures that damaged cells proliferate more slowly than undamaged cells as they expend more energy repairing RT damage
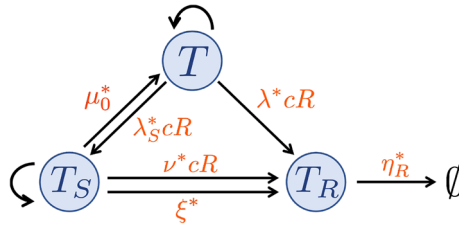
Fig. 1 Schematic showing the interactions between undamaged, damaged and dead tumour cells, T, T_S, T_R, respectively, in response to RT and the proliferation of T and T_S cells as described in the model defined by Eqs. (5)–(9). R denotes the RT dose rate defined by (5) and c denotes the intratumoural oxygen concentration (Colour figure online)

than proliferating. Accordingly, sub-lethally damaged cells consume oxygen for maintenance at a rate proportional to c, with rate constant $q_{1,S}^* = \theta_1 q_1^* > 0$, where $\theta_1 > 1$ as these cells require more energy to repair RT damage. They also consume oxygen for proliferation at a rate proportional to the proliferation rate, with conversion factor $k > 0$ such that $q_{3,S}^* = \frac{q_{2,S}^*}{k}$. Here, we assume the same conversion factor for T and T_S cells, for simplicity. Since $q_{2,S}^* = \theta_2 q_2^*$ and $q_3^* = \frac{q_2^*}{k}$, we also have $q_{3,S}^* = \theta_2 q_3^*$, i.e., damaged cells consume less oxygen for proliferation than undamaged cells. Lastly, as for T cells, T_S cells die from nutrient insufficiency when $c < c_{min}^*$, at a rate proportional to the difference between c and c_{min}^*, with proportionality constant $\delta_{1,S}^* > 0$.

Lethally-damaged cells, T_R, are considered to be dead: their damage cannot be repaired, they do not consume oxygen or proliferate, but they occupy space and are degraded at a constant rate $\eta_R^* > 0$.

One final and important assumption we make is that radiation only affects tumour cells, i.e., we neglect any effects RT may have on tumour angiogenesis, vascular remodelling and injury. This simplifying assumption enables us to focus on elucidating how mechanisms of growth arrest influence one particular type of tumour response to RT, i.e., the cellular response.

2.2 Non-dimensionalisation

We non-dimensionalise Eqs. (5)–(9) by introducing the following scalings:

$$\widehat{T} = \frac{T}{S_{max}}, \quad \widehat{T}_S = \frac{T_S}{S_{max}}, \quad \widehat{T}_R = \frac{T_R}{S_{max}}, \quad \widehat{V}_0 = \frac{V_0}{S_{max}},$$

$$\widehat{c} = \frac{c}{c_{max}^*}, \quad \widehat{R} = \frac{R}{R_{max}}, \quad \widehat{t} = \frac{t}{\tau}.$$

The timescale of interest is the timescale for the duration of RT ($\tau = 1\,\text{min}$). We choose this timescale since we seek to describe the damage and repair associated with RT. The maximum dose rate is also fixed to be $R_{max} = 1\,\text{Gy/min}$ (Konopacka et al. 2016). Then, given that $q_{1,S}^* = \theta_1 q_1^*$, $q_{2,S}^* = \theta_2 q_2^*$ and $q_{3,S}^* = \theta_2 q_3^*$ and dropping hats for notational convenience, we obtain the following dimensionless system:

$$\frac{\mathrm{d}T}{\mathrm{d}t} = q_2 cT(1 - \Sigma) - (\delta_1(c_{min} - c)H(c_{min} - c) + \lambda cR + \nu cR)T + \mu T_S, \tag{10}$$

$$\frac{\mathrm{d}T_S}{\mathrm{d}t} = \theta_2 q_2 cT_S(1 - \Sigma) - (\delta_{1,S}(c_{min} - c)H(c_{min} - c) + \lambda_S cR + \mu + \xi)T_S + \nu cRT, \tag{11}$$

$$\frac{\mathrm{d}T_R}{\mathrm{d}t} = \lambda cRT + (\xi + \lambda_S cR)T_S - \eta_R T_R, \tag{12}$$

$$\frac{\mathrm{d}c}{\mathrm{d}t} = g(1 - c)V_0 - q_1(T + \theta_1 T_S)c - q_3(T + \theta_2 T_S)c(1 - \Sigma), \tag{13}$$

where we have introduced the following dimensionless parameter groupings:

$$q_1 = q_1^* S_{max}\tau, \; q_3 = q_3^* S_{max}^2 \tau, \; q_2 = q_2^* S_{max}^2 c_{max}^* \tau, \; k = \frac{c_{max}^*}{S_{max}} k^*,$$

$$c_{min} = \frac{c_{min}^*}{c_{max}^*}, \; \delta_1 = \delta_1^* c_{max}^* \tau, \; \delta_{1,S} = \delta_{1,S}^* c_{max}^* \tau, \; g = g^* S_{max}\tau, \tag{14}$$

$$\lambda = \lambda^* c_{max}^* R_{max}\tau, \; \lambda_S = \lambda_S^* c_{max}^* R_{max}\tau, \; \nu = \nu^* c_{max}^* R_{max}\tau,$$

$$\mu = \mu^*\tau, \; \xi = \xi^*\tau, \; \eta_R = \eta_R^*\tau.$$

2.3 Defining the Dimensionless Model Parameters

This paper focusses on studying the impact of two distinct growth arrest mechanisms on the qualitative tumour response to RT. We, therefore, fix parameters related to tumour cell responses to RT at the values stated in Table 1. The values of ν, λ, λ_S, μ and η_R are based on values found in the literature (Neira et al. 2020; Steel et al. 1987) and we assume $\lambda = \lambda_S$, for simplicity. We also set $\xi = 5 \times 10^{-4}$ so that cells that undergo mitotic catastrophe have a half-life of approximately 24h. Here, we implicitly assume that the average duration of the cell cycle in healthy cells (Bernard and Herzel 2006) and cancer cells are approximately the same. The parameters that define the RT dosing schedules (e.g., the dose rate, R) are summarised in Sect. 4.1.

Further, we define tumour growth parameters as in our previous work (Colson et al. 2022). In particular, we fix the values of c_{min}, g and k based on parameter values found in the literature and preliminary numerical simulations. For q_1, q_3 and V_0, we consider a biologically realistic range of possible values, motivated by arguments outlined in Colson et al. (2022), as these parameters have a strong influence on the qualitative behaviour of the model in the absence of treatment (see Sect. 3). We make the additional simplifying assumption that, as for the undamaged cells, $\delta_{1,S} = q_{2,S}$. Finally, we set $\theta_1 = 10$ and $\theta_2 = 0.1$ to represent a 10-fold increase in oxygen consumption for maintenance and a 10-fold decrease in oxygen consumption for proliferation in damaged cells.

3 Review of the Key Model Dynamics in the Absence of Treatment

In this section, we summarise the model behaviour in the absence of treatment. Setting $R \equiv 0$ in Eqs. (10)–(13), we recover the dimensionless form of Eqs. (1), (2). In Colson

Table 1 List of dimensionless parameters and their default values

| Parameters	Definition	Value(s)
c_{min}	Anoxic oxygen threshold	10^{-2}
g	Rate of oxygen exchange per unit vascular volume	5
k	Conversation factor	10^{-2}
q_1	O_2 consumption rate for maintenance	$[10^{-2}, 10]$
θ_1	Proportionality constant relating q_1 and $q_{1,S}$	10
q_3	O_2 consumption rate for proliferation	$[10^{-2}, 10]$
q_2	Proliferation rate	kq_3
θ_2	Proportionality constant relating q_2 and $q_{2,S}$ (q_3 and $q_{3,S}$)	0.1
$\delta_1, \delta_{1,S}$	Rates of death due to nutrient insufficiency	$q_2, \theta_2 q_2$
V_0	Vascular volume	$(0, 5 \times 10^{-3}]$
ν	RT sub-lethal damage rate	10
λ, λ_S	RT lethal damage rate	1
μ	Repair rate constant	5×10^{-3}
ξ	Rate of death by mitotic catastrophe	5×10^{-4}
η_R	Clearance rate of cells killed by RT	5×10^{-5}
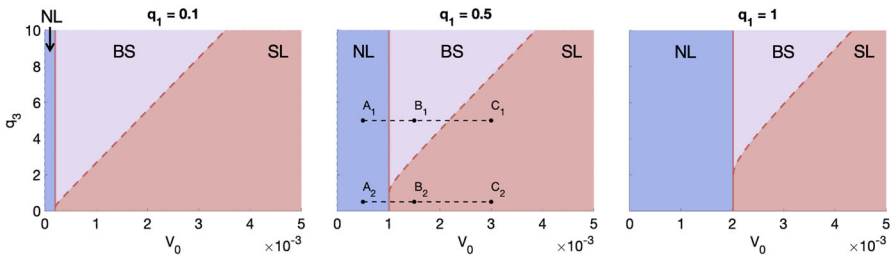
Fig. 2 For $q_1 \in \{0.1, 0.5, 1\}$, we show the regions of (V_0, q_3)-space in which only the stable NL steady state exists (blue), only the stable SL steady state exists (red) and both the stable NL and SL steady states co-exist (purple). The solid and dashed red lines represent the boundaries between the three regions. For $q_1 = 0.5$, the points A_1–C_1 correspond to $(V_0, q_3) \in \{(0.0005, 5), (0.0015, 5), (0.003, 5)\}$, respectively, and A_2–C_2 to $(V_0, q_3) \in \{(0.0005, 0.5), (0.0015, 0.5), (0.003, 0.5)\}$, respectively. Tumours defined by parameter sets A_1–C_1 have values of q_3 which are sufficiently larger than q_1 so that there is bi-stability, while, for A_2–C_2, bistability does not occur (Colour figure online)

et al. (2022), we showed that this model admits two non-trivial, stable steady states (see Appendix A): (i) a nutrient limited (NL) steady state, attained when cell proliferation balances cell death due to nutrient starvation; (ii) a space limited (SL) steady state, attained when cell proliferation ceases due to lack of space, with no cell death.

For these solutions to be physically realistic and lie in the appropriate nutrient regime, they must satisfy $0 \leq T \leq 1 - V_0$ and either $0 \leq c < c_{min}$ (for the NL steady state) or $c \geq c_{min}$ (for the SL steady state). Imposing these conditions, we find that admissible NL and SL steady state solutions lie in different regions of parameter space. These regions are defined by the values of q_1, q_3 and V_0, with no qualitative changes when c_{min} and g vary (Colson et al. 2022). Figure 2 depicts these regions in (q_3, V_0)-space for three values of q_1 and fixed values of $c_{min} = 0.01$ and $g = 5$.

Given q_1, there exists a threshold value of V_0, which we denote by V_N, which is independent of q_3, such that only NL steady states exist for $0 < V_0 \leq V_N$. Tumours in this region of parameter space (e.g., A_1 and A_2) are said to be in a NL growth regime. Further, given q_1, and for q_3 sufficiently large relative to q_1, there exists another threshold value of V_0, which we denote by V_S, such that only SL steady states exist for $V_0 \geq V_S > V_N$. Tumours in this region (e.g., C_1, B_2 and C_2) are said to be in a SL growth regime. Further, where $V_N < V_0 < V_S$, the NL and SL steady states co-exist. A tumour in this region (e.g., B_1) may evolve to either steady state, depending on its initial conditions. We consider such tumours to be in a bistable (BS) growth regime. Finally, for $q_3 \lesssim q_1$, we have that, for $V_0 > V_N$, a unique steady state exists and it is of SL type.

Figure 3 shows the time evolution of the tumour cell volume, T, and the intra-tumoural oxygen concentration, c, and the corresponding bifurcation diagrams for tumours A_1–C_1 and A_2–C_2. In all cases, the NL steady state values for T and c (T^* and c^*, respectively) are smaller than the SL ones. This is consistent with the assumption that, in the absence of angiogenesis, well-oxygenated tumours attain larger volumes than poorly-oxygenated tumours. Further, tumours in a BS regime evolve to their NL steady state for initial conditions satisfying $0 < T(0) \ll T^*$, which we use to simulate tumour growth. As the values of T^* and c^* for NL tumours increase with V_0, tumours
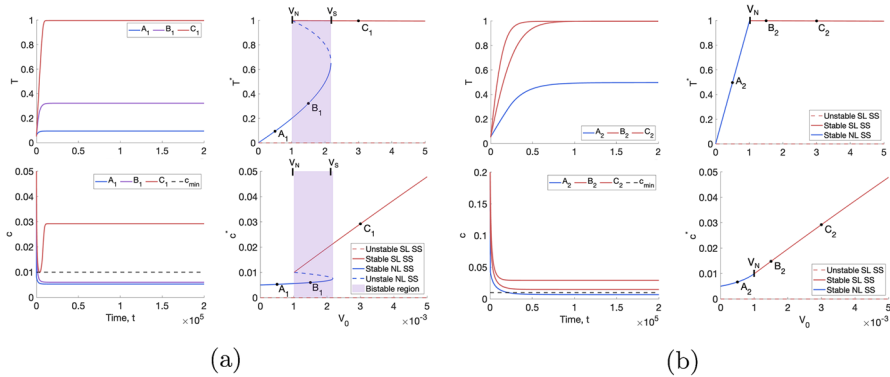
Fig. 3 With $R \equiv 0$, we numerically solve Eqs. (10)–(13) for $t \in (0, 2 \times 10^5]$ subject to the initial conditions $(T(0), T_S(0), T_R(0), c(0)) = (0.05, 0, 0, 1)$ and plot the evolution of the tumour volume and oxygen concentration in time. In (**a**), (q_1, q_3, V_0) correspond to points A_1–C_1 in Fig. 2 and, in (**b**), they correspond to points A_2–C_2. The remaining model parameters are fixed at the default values in Table 1. The bifurcation diagrams show how the steady state values for T and c change as V_0 varies for (q_1, q_3) corresponding to A_1–C_1 in (**a**) and for (q_1, q_3) corresponding to A_2–C_2 in (**b**). In both cases, the NL steady state increases with V_0 and is smaller than the SL steady state, which decreases with V_0. The tumour in a BS regime (B_1) grows to its NL steady state (Colour figure online)

in a BS regime will grow to larger volumes than tumours in a NL regime (and smaller volumes than tumours in a SL regime). We also note that, in BS regimes, there is a large jump in T^* and c^* at V_S, the threshold value of V_0 separating the BS and SL regimes. In contrast, in monostable regimes, T^* and c^* depend continuously on V_0.

In summary, in the absence of treatment (i.e., $R \equiv 0$), Eqs. (10)–(13) describe three possible scenarios for tumour growth: (i) nutrient limited growth, where the tumour grows to a NL steady state at which proliferation balances cell death due to nutrient insufficiency; (ii) space limited growth, where the tumour grows to a SL steady state at which proliferation ceases due to space constraints; (iii) bistable growth, where a tumour grows to a NL steady state given physically realistic initial conditions $(0 < T(0) \ll T^*)$. *In vivo*, we expect that tumours growing in poorly-perfused regions (e.g., breast, bone) and/or that elicit a weaker angiogenic response would be in the NL regime, while tumours growing in well-perfused regions (e.g., lung, liver, brain) and/or that elicit a stronger angiogenic response would be in the SL regime. Tumours growing in well-perfused regions that are highly proliferative and, therefore, more likely to outgrow their nutrient supply, would be in the BS regime. In Sect. 4, we investigate how tumours in these three growth regimes respond to RT.

4 Investigating Tumour Response to Radiotherapy

4.1 Methods

Our aim is to understand the qualitative response of tumours in nutrient limited (NL), space limited (SL) and bistable (BS) regimes to a range of fractionated radiotherapy

(RT) treatments. As a first step, we create three virtual tumour populations as follows. We first fix all tumour growth model parameters, except q_1, q_3 and V_0, at the default values stated in Table 1. We then also fix $V_0 = 0.0005$, $V_0 = 0.005$ and $V_0 = 0.00275$ for tumours in the virtual NL, SL and BS regimes, respectively. Allowing q_1 and q_3 to vary, we generate three virtual tumour populations of size $N = 250$ by randomly selecting N (q_1, q_3) pairs, corresponding to the NL, SL and BS regimes, respectively. Each pair is formed by sampling pairs of values of q_1 and q_3 from uniform distributions whose lower and upper bounds depend on the growth regime (NL, SL or BS), the value of V_0 and, for sampling q_3 in the BS and SL regimes, the value of q_1 (see Appendix B).

We then define the RT protocols of interest. We vary the dose amount $D \in [\![0, 5]\!]$ (Gy) and the number of doses per week $N_{frac} = \{1, 3, 5\}$. We assume that each dose is administered in $\delta_R = 10$ min and, therefore, we vary the dimensionless dose rate, $R := \frac{D}{\delta_R R_{max}} \in \{0.1, 0.2, 0.3, 0.4, 0.5\}$. We also suppose that all fractions are applied at the same time of day and the first weekly fraction is applied on Mondays, with subsequent fractions applied at equally spaced time intervals during Monday to Friday (e.g., 3 doses per week corresponds to doses on Monday, Wednesday and Friday). Further, the duration of each fractionation schedule is determined so that the total dose administered is 80 Gy (or the closest multiple of D to 80 Gy).

For each set of tumours and each RT protocol, we solve Eqs. (10)–(13) numerically for $t \in (0, t^*]$, $t^* > 0$, using ODE45, a single step MATLAB built-in solver for non-stiff ODEs that is based on an explicit Runge–Kutta (4,5) formula, the Dormand-Prince pair (Dormand and Prince 1980). (The code is available at: https://github.com/chloeacolson/InvestigatingTumourResponsesRadiotherapy.) For simplicity, we impose the initial conditions

$$(T, T_S, T_R, c) = (T^*, 0, 0, c^*), \tag{15}$$

where T^* and c^* are, respectively, the steady state tumour volume and oxygen concentration in the absence of treatment. All RT parameters are fixed at the default values listed in Table 1.

For each simulation, we record $\bar{T}$, $\bar{T}_S$ and $\bar{T}_R$, the mean undamaged, damaged and dead cell volumes in the last week of treatment, respectively. We also define the percent change in (mean) viable and total cell volumes between the start and the end of treatment as follows

$$\Delta_{\text{viable}} := 100 \times \frac{(\bar{T} + \bar{T}_S) - T_0}{T_0} \quad \text{and} \quad \Delta_{\text{total}} := 100 \times \frac{\bar{\Sigma} - \Sigma_0}{\Sigma_0}, \tag{16}$$

where

$$\Sigma_0 = T_0 + V_0, \quad \Sigma = T + T_S + T_R + V_0.$$

We also quantify the end-of-treatment tumour composition (relative to the total tumour volume at the start of treatment) as follows

$$\%T := 100 \times \frac{\bar{T}}{\Sigma_0}, \quad \%T_S := 100 \times \frac{\bar{T}_S}{\Sigma_0}, \quad \%T_R := 100 \times \frac{\bar{T}_R}{\Sigma_0} \quad \text{and}$$

$$\% V_0 := 100 \times \frac{V_0}{\Sigma_0}. \tag{17}$$

We note that the variables defined in (17) can be used to describe $\Delta_{total} = (\%T + \%T_S + \%T_R + \%V_0) - 100$. Henceforth, for brevity, we refer to the relative changes in tumour cell volumes, as defined in (16) and (17), as changes in tumour cell volumes. Finally, we record $\bar{c}$, the mean oxygen concentration in the last week of treatment, and the post-treatment steady state values of all the dependent variables.

4.2 Characterising Tumour Response to Fractionated RT

In this section, we investigate the response of tumours in the NL, SL and BS virtual populations to fractionated RT. For each regime, we initially study tumour response to a conventional fractionation schedule consisting of 5×2 Gy fractions per week for 8 weeks. In particular, we determine the average response and explore how certain values of q_1, q_3 and V_0 generate extremal behaviour. We also study the impact of the dose and dosing frequency on tumour response. We consider monostable regimes before looking at the bistable regime.

4.2.1 Tumours in Monostable Regimes: The NL and SL Virtual Tumour Populations

Typical responses to a conventional fractionation schedule. Fig. 4 shows the response of two NL and SL tumours to RT, both of which experience a decrease in viable tumour cell volume, $T + T_S$, during treatment. Since, in both cases, the dependent variables evolve to time periodic solutions within 5 weeks of treatment, we deduce that there is a maximal reduction in the viable cell volume that can be achieved with this fractionation schedule. This maximum reduction, which we quantify using Δ_{viable}, is significantly larger for the SL tumour at approximately 37.6% than for the NL tumour at approximately 4.36%. RT is more effective for the SL tumour as it is better oxygenated than the NL tumour and, hence, it experiences a higher rate of RT cell kill and greater accumulation of dead material, T_R, than the NL tumour.

Figure 4 also shows that, for both tumours, the oxygen concentration and the viable tumour cell volume decrease when RT is applied. This is because T and T_S cells consume oxygen at different rates: we recall that the oxygen consumption rates of sub-lethally damaged cells satisfy $q_{1,S} = 10q_1$ and $q_{3,S} = 0.1q_3$. Therefore, changes in tumour composition during treatment will alter the overall oxygen consumption rate of viable tumour cells, leading to transient, or persistent, increases or decreases in the oxygen concentration depending on the values of q_1 and q_3.

Figure 5 shows the distributions of Δ_{viable} and Δ_{total}, following a conventional fractionation schedule, across the NL and SL virtual populations. We note that the behaviour shown in Fig. 4 for specific NL and SL tumours is representative of the average behaviour of each virtual population. In particular, tumours in the SL cohort typically respond well to treatment, with median and $(Q1, Q3)$ values of Δ_{viable} equal to -37.9 and $(-30.7, -54.1)$, respectively, and $\Delta_{total} < 0$ across the virtual population. Given the initial conditions (15), the latter follows because SL tumours fully occupy the available space at the start of treatment. Tumours in the NL cohort
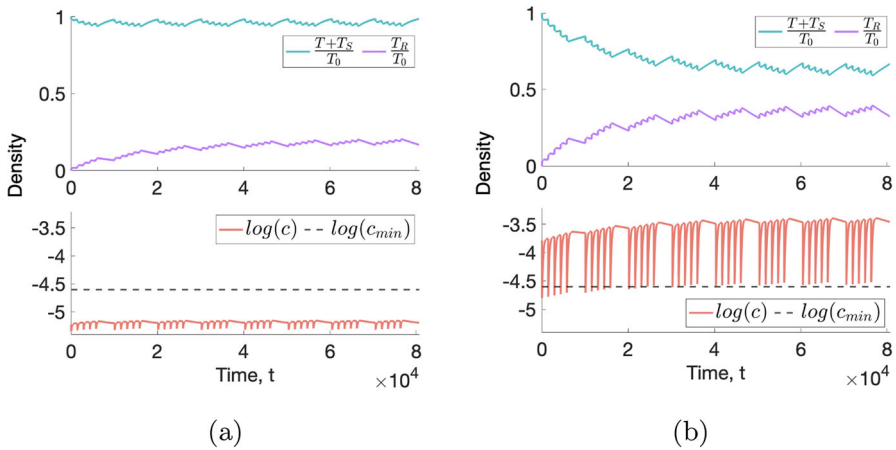
Fig. 4 For a conventional fractionation schedule, we numerically solve Eqs. (10)–(13) for $t \in (0, 8 \times 10^4]$ subject to the initial conditions (15). In (**a**), we set $(q_1, q_3, V_0) = (0.832, 2.98, 0.0005)$, which corresponds to a NL tumour. In (**b**), we set $(q_1, q_3, V_0) = (1.08, 8.83, 0.005)$, which corresponds to a SL tumour. Although both tumours exhibit a decrease in viable cell volume, RT cell kill and accumulation of dead material is more significant for the SL than the NL tumour for this choice of parameter values (Colour figure online)
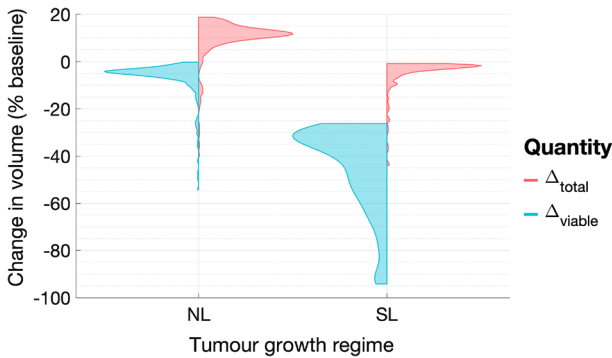
Fig. 5 For virtual cohorts of NL and SL tumours, the violin plots show the distributions of Δ_{viable} and Δ_{total}. The viable cell volume of all NL and SL tumours decreases during RT, with SL tumours showing significantly greater percentage changes. The total volume decreases for all SL tumours, while it increases for most NL tumours. We identify several outliers, which exhibit significantly larger reductions in their viable and total cell volumes (Colour figure online)

typically respond less well to treatment, with larger median and $(Q1, Q3)$ values of Δ_{viable} equal to -4.57 and $(-3.52, -6.53)$, respectively, and $\Delta_{total} > 0$, for at least 90% of tumours. When the net RT-induced cell death is minimal, NL tumours, which do not occupy all available free space at the start of treatment, can grow larger due to increases in the dead cell volume. We also note that the value of $\Delta_{total} - \Delta_{viable}$ is larger for SL tumours since they accumulate more dead material.

In both regimes, we observe outliers, which undergo much larger reductions in $T + T_S$ and Σ than the average tumour. This suggests that certain parameter values
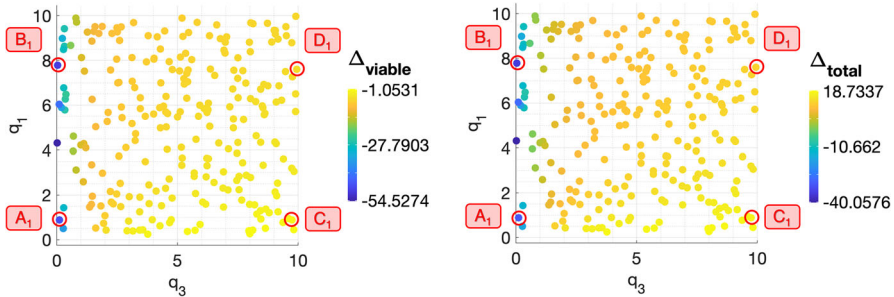
Fig. 6 The scatter plots show the values of Δ_{viable} and Δ_{total}, following a conventional fractionation schedule, for each (q_1, q_3) pair used to generate the set of virtual NL tumours. Δ_{viable} and Δ_{total} increase with q_3 and decrease with q_1 (Colour figure online)

within the NL and SL regimes correspond to tumours which are more sensitive to RT than the average NL and SL tumour.

The influence of the oxygen consumption rates**, q_1 **and** q_3, **on treatment outcome following a conventional fractionation schedule. We now investigate the role of q_1 and q_3 in tumour response to RT. The scatter plots in Fig. 6 show the values of Δ_{viable} and Δ_{total} across the (q_1, q_3) pairs which define the NL virtual population. The response of NL tumours is most sensitive to the value of q_3, with smaller values leading to greater reductions in viable and total cell volumes. Further, higher values of q_1 are also associated with larger reductions in viable and total cell volumes. To understand these findings, we study the response to RT of four representative tumours corresponding to (q_1, q_3) sets, A_1, B_1, C_1 and D_1 (see Fig. 6 and Table 2).

Comparing the response of tumours A_1 and B_1 to tumours C_1 and D_1 in Fig. 7a, we see that a smaller value of q_3 implies higher average oxygen levels and slower cell proliferation (since $q_2 = 0.01q_3$). We conclude that two mechanisms could explain the increased efficacy of RT for low values of q_3: (i) higher rates of RT cell kill due to increased oxygenation or (ii) limited regrowth between RT fractions due to decreased proliferation.

While oxygen levels are higher in tumours A_1 and B_1 than tumours C_1 and D_1, respectively, when RT is applied (see Fig. 7a), their values of $\%T_R$ are slightly smaller (16.65% (A_1) vs. 18.42% (C_1) and 13.79% (B_1) vs. 16.29% (D_1); see Fig. 7b). This suggests that the net increase in oxygen levels when values of q_3 are small does not significantly impact the rates of cell kill due to RT. By contrast, Fig. 7a shows that the relative increase in the viable cell volume of tumours A_1 and B_1 between fractions is marginal, whereas the relative increase in the viable cell volume of tumours C_1 and D_1 between fractions is sufficiently large for it to return to its initial volume over the weekend break from RT. This indicates that the value of q_3 impacts the reduction in the tumour burden by modulating tumour regrowth between fractions (rather than by increasing RT-induced cell death).

Figure 7b also shows that a larger value of q_1 can slightly increase the magnitude of the reductions in Δ_{viable} and Δ_{total}. Since high values of q_1 lead to lower average oxygen levels (Fig. 7a), RT cell kill rates are smaller, while the rate of cell death due to hypoxia is larger than for low values of q_1. The balance between these two processes
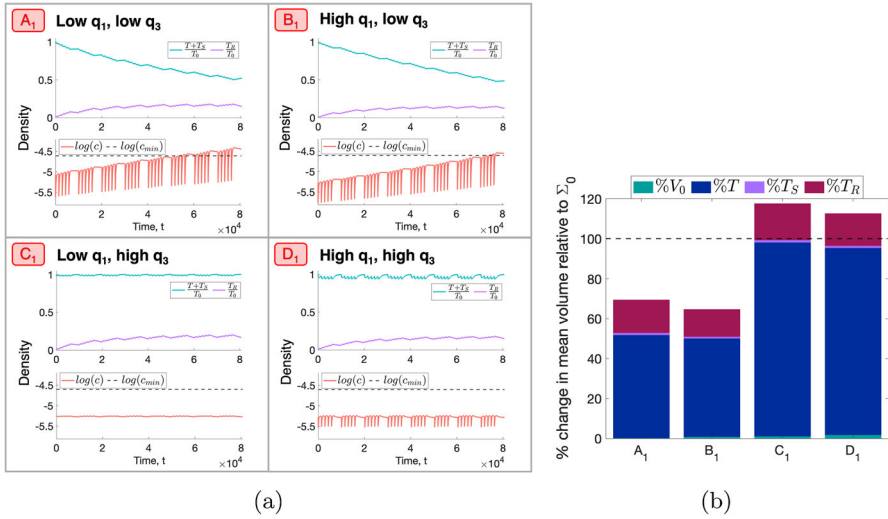
Fig. 7 (**a**) For a conventional fractionation schedule, we numerically solve Eqs. (10)–(13) for $t \in (0, 8 \times 10^4]$ subject to the initial conditions (15). In $A_1 - D_1$, we fix $V_0 = 0.0005$ and (q_1, q_3) as indicated by the points A_1, B_1, C_1 and D_1 in Fig. 6, which correspond to NL tumours. (**b**) Bar graph showing the mean composition of tumours $A_1 - D_1$ in the last week of a conventional fractionation schedule, where $\%T$, $\%T_S$, $\%T_R$ and $\%V_0$ are defined in Eq. (17). Tumours with small values of q_3 (A_1, B_1) undergo sustained reductions in $T + T_S$ during treatment, leading to larger reductions in total volume. Tumours with large values of q_3 (C_1, D_1) experience transient reductions in $T + T_S$ as they regrow to their initial volume during the weekend break from RT, and their total volume increases as they accumulate dead material. A high value of q_1 (B_1, D_1) leads to a modest improvement in the tumour response, but does not yield a large reduction in tumour volume (Colour figure online)

Table 2 Parameter sets A_1, B_1, C_1 and D_1 corresponding to the representative NL tumours

Tumour	q_1	q_3
A_1	8.91×10^{-1}	1.14×10^{-1}
B_1	7.78	4.01×10^{-2}
C_1	8.91×10^{-1}	9.75
D_1	7.60	9.94

determines whether cell death increases or decreases as q_1 increases. For tumours C_1 and D_1, Fig. 7a shows that the reduction in $T + T_S$ following RT is greater and the increase in T_R is smaller for larger values of q_1. This confirms that a larger reduction in tumour burden can be achieved for large values of q_1 despite a reduction in RT-induced cell death: in such cases, increased cell death due to hypoxia drives the reduction in tumour volume.

Overall, we have shown that both low values of q_3 and high values of q_1 characterise the best NL responders. Since Fig. 7a, b suggest that the value of q_1 has a less significant influence on tumour reduction than q_3, we conclude that growth limitation between RT fractions, rather than high rates of cell death due to RT or oxygen insufficiency, has the greatest influence on the efficacy of RT for NL tumours.
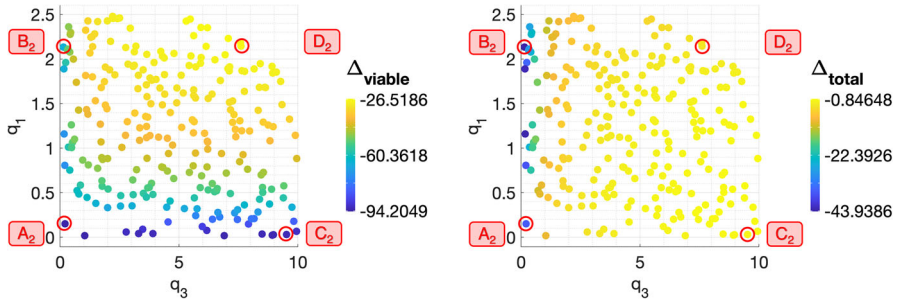
Fig. 8 The scatter plots show the values of Δ_{viable} and Δ_{total}, following a conventional fractionation schedule, for the (q_1, q_3) pairs used to generate the set of virtual SL tumours. Smaller values of Δ_{viable} are obtained for low values of q_1 and/or q_3, while smaller values of Δ_{total} are obtained for low values of q_3 (Colour figure online)

Table 3 Parameter sets A_2, B_2, C_2 and D_2 corresponding to the representative SL tumours

Tumour	q_1	q_3
A_2	1.51×10^{-1}	2.10×10^{-1}
B_2	2.14	1.43×10^{-1}
C_2	3.21×10^{-2}	9.53
D_2	2.14	7.61

Figure 8 shows the values of Δ_{viable} and Δ_{total} across the (q_1, q_3) pairs which define the SL virtual population. The response of SL tumours is sensitive to the values of both q_1 and q_3: greater reductions in viable cell volume are obtained for smaller values of q_1 and/or q_3, while greater reductions in total cell volume are obtained for smaller values of q_3. To understand these results, we study the response to RT of tumours corresponding to four representative (q_1, q_3) sets A_2, B_2, C_2 and D_2 (see Fig. 8 and Table 3).

Figures 9a, b reveal that A_2 and C_2 accumulate a larger number of dead cells than tumours B_2 and D_2. This difference in tumour composition is amplified during treatment and the parameter which influences this distinction most is q_1. Figure 9a shows that for low values of q_1 (tumours A_2 and C_2), the intratumoural oxygen concentration, c, is at least 10-fold higher than for high values of q_1 (tumours B_2 and D_2). In particular, $c \gg c_{min}$ throughout treatment when q_1 is small, which means that there is no cell death due to nutrient insufficiency and cell death is solely attributable to RT. Therefore, the decrease in viable cell volume (and corresponding increase in dead cell volume) in tumours A_2 and C_2 following each RT fraction is driven by cell kill due to RT, which is enhanced by low values of q_1.

For tumours B_2 and D_2, Fig. 9a also shows that, even though the oxygen concentration transiently drops below c_{min} when each RT fraction is applied, there is a net increase in c throughout treatment and, in particular, the weekly average oxygen concentration remains above c_{min} (result not shown). Therefore, we expect RT cell kill to increase during the fractionation schedule and cell death due to hypoxia to decrease. Since RT cell kill remains limited by low oxygen levels for both tumours, neither of the
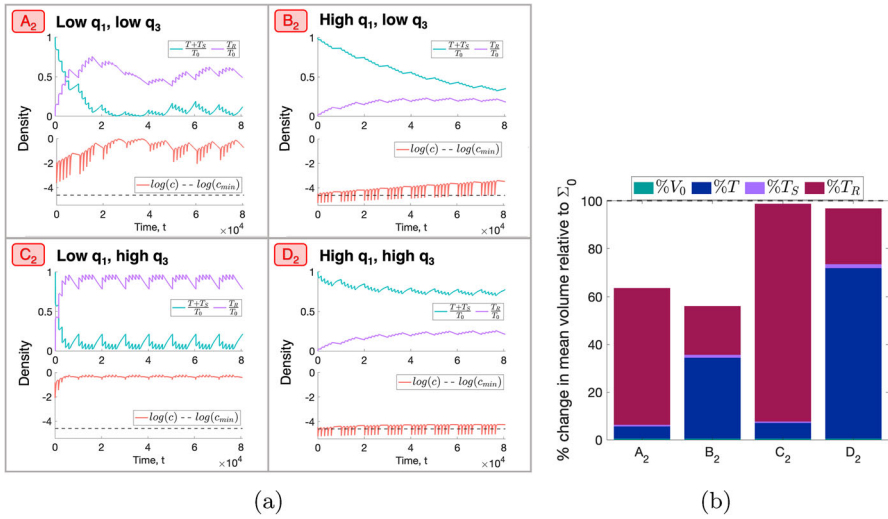
Fig. 9 (**a**) For a conventional fractionation schedule, we numerically solve Eqs. (10)–(13) for $t \in (0, 8 \times 10^4]$ subject to the initial conditions (15). In A_2–D_2, we fix $V_0 = 0.005$ and (q_1, q_3) as indicated by the points A_2, B_2, C_2 and D_2 in Fig. 8, which correspond to SL tumours. (**b**) Bar graph showing the mean composition of tumours A_2–D_2 in the last week of a conventional fractionation schedule, where $\%T$, $\%T_S$, $\%T_R$ and $\%V_0$ are defined in Eq. (17). We observe three qualitative behaviours: (i) low q_1 (A_2, C_2) is associated with high oxygen levels, high rates of RT cell kill and a large accumulation of dead cell material; (ii) high q_1 and low q_3 (B_2) implies a smaller reduction in viable volume due to smaller RT cell kill and a greater reduction in total volume due to limited inter-fraction tumour growth and smaller dead cell accumulation; (iii) high q_1 and q_3 (D_2) leads to modest reductions in viable and total volumes due to low rates of RT cell kill and high rates of cell proliferation. Overall, the values of q_1 and q_3 influence the tumour composition and the total tumour volume, respectively (Colour figure online)

two proposed cell death mechanisms is responsible for the increased RT efficacy for tumour B_2 compared to tumour D_2. However, Fig. 9a reveals that the relative increase in $T + T_S$ between fractions is smaller for tumour B_2, which is characterised by low q_3. We, therefore, conclude that the increased RT efficacy is driven by reduced tumour regrowth between fractions (similarly to NL tumours with low q_3).

Figure 9b further shows how low values of q_3 enable greater reductions in total tumour volume, Σ. Since, for tumours B_2 and D_2, the values of $\%T_R$ are comparable while the value of $\%T$ is smaller for tumour B_2, the larger reduction in Σ observed for tumour B_2 is due to increased net cell death (as described above). In contrast, for tumours A_2 and C_2, the values of $\%T$ are comparable while the value of $\%T_R$ is smaller for tumour A_2. The larger reduction in Σ observed for tumour A_2 is, therefore, due to a smaller accumulation of dead material, which occurs when lower viable cell volumes (caused by slower tumour regrowth between fractions) and/or lower oxygen levels reduce RT-induced cell death.

Overall, we have shown that two mechanisms can contribute to the increased efficacy of RT for certain tumours in a SL regime. These mechanisms are cell death due to RT and limited tumour regrowth between RT doses. Their relative contributions depend on the values of q_1 and q_3. More specifically, when q_1 is small, RT cell kill is the dominant mechanism contributing to increased net cell death and, when q_3
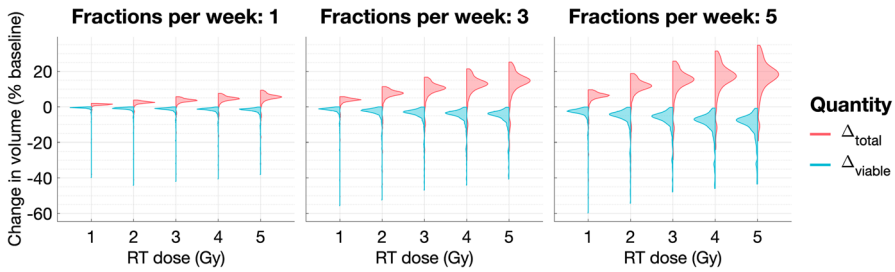
Fig. 10 For the virtual NL population, we show how the distributions of Δ_{viable} and Δ_{total} change as the dose rate, $R \in \{0.1, 0.2, 0.3, 0.4, 0.5\}$, and the number of fractions per week, $N_{frac} \in \{1, 3, 5\}$, vary. The mean value of Δ_{viable} decreases, while the mean values of Δ_{total} and $\Delta_{total} - \Delta_{viable}$ increase as R and N_{frac} increase (Colour figure online)

is also small, limited regrowth between fractions ensures a larger reduction in total tumour volume. When q_1 is large and q_3 is small, limited regrowth between fractions determines the response to RT by ensuring larger reductions in viable and total cell volumes.

The effect of the dosing schedule on typical tumour response. We now consider how, for a fixed total dose, the dose rate, R, and the number of fractions per week, N_{frac}, affect tumour response to RT. For the virtual cohorts of NL and SL tumours, Figs. 10 and 11, respectively, show the distributions of Δ_{viable} and Δ_{total} for fractionation schedules with $R \in \{0.1, 0.2, 0.3, 0.4, 0.5\}$ and $N_{frac} \in \{1, 3, 5\}$. For NL tumours, the mean reduction in viable volume and the difference between the viable and total volumes increase with R and N_{frac}. However, the maximum reduction in viable and total volumes typically decreases with R (for fixed N_{frac}), and the mean and maximum increases in total volumes also increase with R and N_{frac}. Therefore, a higher dosing frequency and/or dose may not lead to greater RT efficacy for tumours in the NL regime. By contrast, for SL tumours, on average, the reduction in the viable and total volumes and the difference between the viable and total volumes increase with R and N_{frac}. The response of SL tumours is, thus, consistent with the current, standard approach to RT protocol design, which aims to maximise RT cell kill by applying the highest tolerable total dose, in sufficiently frequent fractions, to the tumour. This result is also supported by other modelling approaches, e.g., Lewin et al. (2018) developed a spatially resolved model of avascular tumour growth and RT cell death which predicted that there is a minimum RT dose, for a fixed dosing frequency, and a minimum dosing frequency, for a fixed RT dose, below which tumours grow during treatment.

4.2.2 Tumours in the Bistable Regime

Typical response to a conventional fractionation schedule. Figure 12a shows the average response of a tumour in a BS regime to a conventional fractionation schedule. RT has a detrimental effect as tumour regrowth between fractions and over the weekend outweighs RT-induced cell death. The dead cell volume also increases throughout treatment, implying an increase in total volume. Figure 12b further shows that, for the
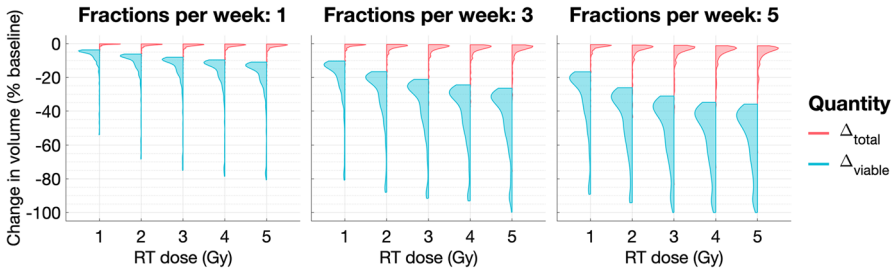
Fig. 11 For the virtual SL population, we show how the distributions of Δ_{viable} and Δ_{total} change as the dose rate, $R \in \{0.1, 0.2, 0.3, 0.4, 0.5\}$, and the number of fractions per week, $N_{frac} \in \{1, 3, 5\}$, vary. The mean values of Δ_{viable} and Δ_{total} decrease, while the mean value of $\Delta_{total} - \Delta_{viable}$ increases as R and N_{frac} increase (Colour figure online)
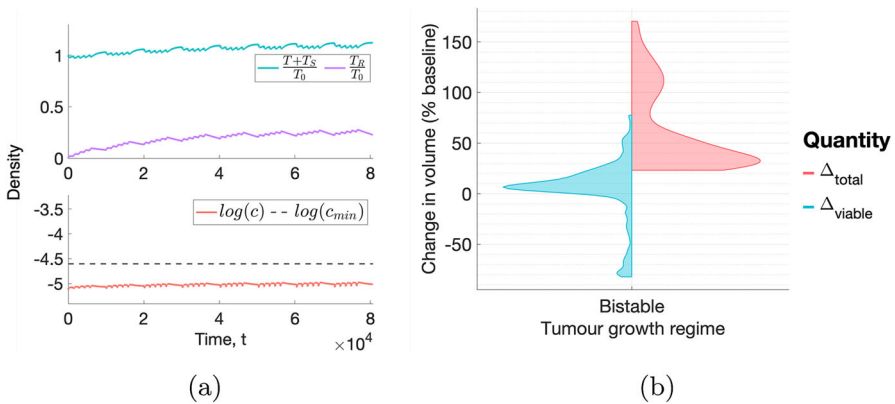

Fig. 12 (**a**) For a conventional fractionation schedule, we numerically solve Eqs. (10)–(13) for $t \in (0, 8 \times 10^4]$ subject to the initial conditions (15). We set $(q_1, q_3, V_0) = (0.787, 8.38, 0.00275)$. This tumour represents the typical behaviour in a BS regime. (**b**) Violin plots representing the distributions of Δ_{viable} and Δ_{total}. While the effect of RT is deleterious for most tumours, with several outliers experiencing larger than average increases in viable and total volumes, there are tumours that exhibit larger than average decreases in viable volume (Colour figure online)

BS virtual cohort, $\Delta_{viable} > 0$ for at least 80% of tumours and $\Delta_{total} > 0$ for all tumours. This reveals that most tumours in the BS virtual cohort respond badly to RT.

The results in Fig. 12b also indicate that a few virtual tumours are more or less sensitive to RT than the average tumour in the BS virtual population: while their total volume increases during RT, their viable volume undergoes a $20 - 80\%$ decrease or $40 - 80\%$ increase, respectively, by the end of treatment. We investigate the response to RT of these outliers in more detail in the following section.

The influence of q_1, q_3 ***and*** V_0 ***on treatment outcome following a conventional fractionation schedule.*** As for tumours in monostable regimes, we study the influence of q_1 and q_3 on tumour response to RT, but we also study the role played by the vascular volume, V_0. More specifically, we introduce a function V_d, which quantifies how close
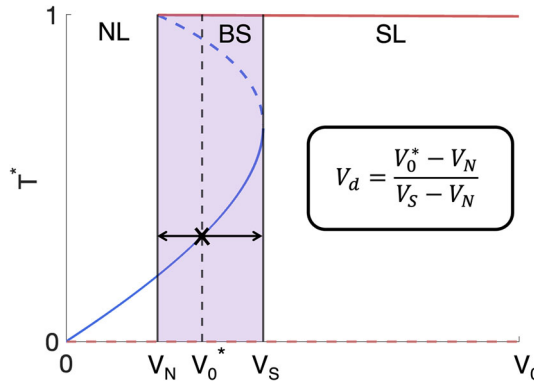
Fig. 13 Schematic bifurcation diagram showing how, for fixed values of q_1 and q_3, the steady state value of the tumour cell volume, T^*, changes with V_0. The shaded purple region represents the bistable region, where V_N and V_S are the threshold values of V_0 below and above which only NL and SL steady states exist, respectively. For tumours with $V_N < V_0^* < V_S$, we define V_d by (18) to quantify the relative proximity of $T^*(V_0^*)$ to the monostable NL and SL regions (Colour figure online)

a tumour in the BS regime lies to the NL and SL regimes (see the schematic in Fig. 13):

$$V_d(V_0) = \frac{V_0 - V_N}{V_S - V_N},$$ (18)

where V_N and V_S are the threshold values of V_0 below and above which only NL and SL steady states exist, respectively. Further,

$$\begin{cases} V_d \to 0 \text{ as } V_0 \to V_N, \\ V_d \to 1 \text{ as } V_0 \to V_S. \end{cases}$$ (19)

In particular, $V_d \gtrsim 0$ for tumours which are close to the NL regime, whereas $V_d \lesssim 1$ for tumours which are close to the SL regime.

The scatter plots in Fig. 14 show the values of Δ_{viable} and Δ_{total} across the (q_1, q_3) and (q_1, V_d) pairs corresponding to the BS virtual population. We note that the values of q_3 and V_d are correlated: for fixed q_1, the lowest value of V_d corresponds to the highest value of q_3 and vice versa. It is, therefore, sufficient to describe the response of tumours in a BS regime with respect to the values of q_1 and V_d. The largest reductions in viable volume are obtained for lower values of q_1 and $V_d \lesssim 1$, whereas the largest increases in viable volume are obtained for higher values of q_1 and intermediate values of V_d. Those tumours with the smallest and largest values of Δ_{viable} also undergo the largest increases in total volume: for intermediate to high values of V_d, Δ_{total} decreases as V_d and q_1 increase.

We now select four representative (q_1, q_3, V_d) sets A_3, B_3, C_3 and D_3 (see Fig. 14 and Table 4) and study the corresponding tumours' response to RT. Figures 15a, b show that tumours A_3 and B_3 decrease in viable volume, with A_3 experiencing a larger than average reduction, while C_3 and D_3 increase in viable volume, with C_3 experiencing
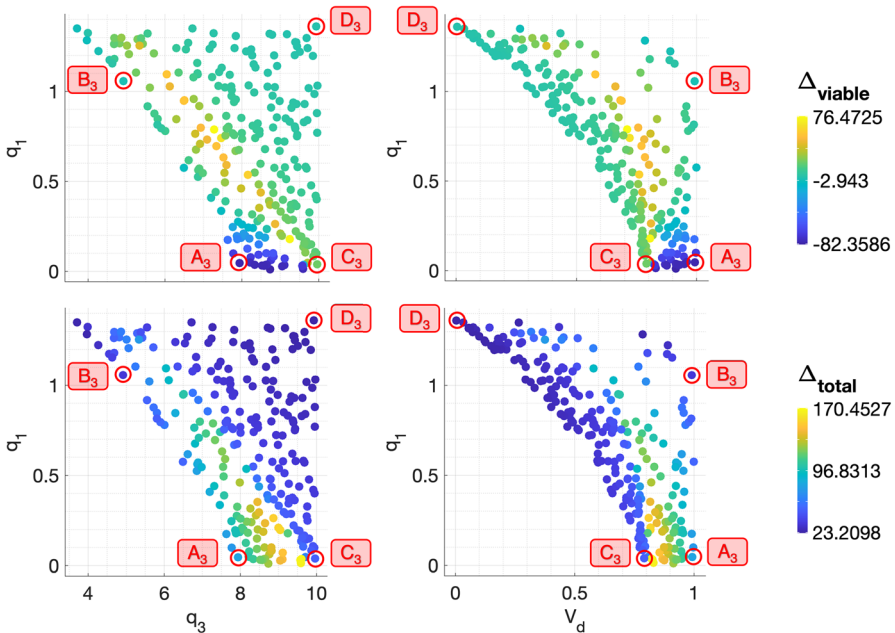
Fig. 14 The scatter plots show the values of Δ_{viable} and Δ_{total}, following a conventional fractionation schedule, for the (q_1, q_3) and (q_1, V_d) pairs used to generate the set of virtual tumours in a BS regime. The smallest values of Δ_{viable} are associated with lower values of q_1 and q_3 and $V_d \lesssim 1$, while the largest values of Δ_{viable} are associated with higher values of q_1, lower values of q_3 and intermediate values of V_d. Δ_{total} is largest for the tumours with the smallest and largest values of Δ_{viable} (Colour figure online)

Table 4 Parameter sets A_3, B_3, C_3 and D_3 corresponding to the representative tumours in the BS cohort

Tumour	q_1	q_3	V_d
A_3	4.55×10^{-2}	7.94	0.993
B_3	1.06	4.92	0.991
C_3	3.92×10^{-2}	9.96	0.791
D_3	1.36	9.93	0.00376

a larger than average increase. While tumours A_3 and C_3 have low q_1, $V_d \approx 1$ for A_3 and $V_d \approx 0.8$ for C_3. Similarly, while tumours B_3 and D_3 have high q_1, $V_d \approx 1$ for B_3 and $V_d \approx 0$ for D_3. Given (19), this suggests that the behaviour of tumours in a BS regime that lie sufficiently close to the SL or NL regions will be, respectively, similar to that of SL or NL tumours with values of q_1 and q_3 of the same order of magnitude.

More specifically, tumours A_3 and B_3 respond to RT similarly to SL tumours C_2 and D_2, respectively (recall Fig. 9a, b), while tumour D_3 responds similarly to NL tumour D_1 (recall Fig. 7a, b). For tumour A_3, this response involves an initial large increase in viable and total volume as the tumour evolves towards its SL steady state, followed by a substantial increase in RT cell kill, the average oxygen concentration and the dead cell volume. Despite the reduction in viable volume, the accumulation of dead material implies a significant increase in total volume. The same qualitative
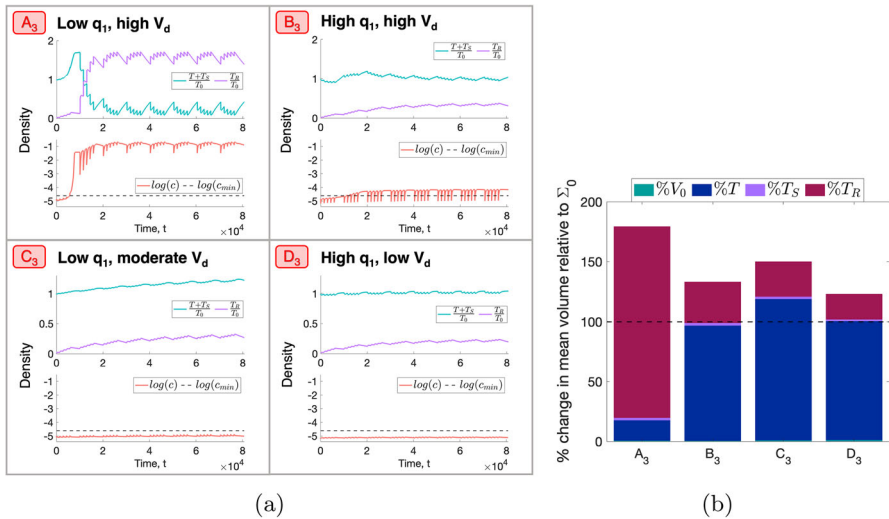
Fig. 15 (**a**) For a conventional fractionation schedule, we numerically solve Eqs. (10)–(13) for $t \in (0, 8 \times 10^4]$ subject to the initial conditions (15). In A_3-D_3, we fix $V_0 = 0.00275$ and (q_1, q_3) as indicated by the points A_3, B_3, C_3 and D_3 in Fig. 14. (**b**) Bar graph showing the mean composition of tumours A_3-D_3 in the last week of a conventional fractionation schedule, where $\%T$, $\%T_S$, $\%T_R$ and $\%V_0$ are defined in Eq. (17). A_3 and B_3 decrease in viable volume and increase in total volume, while C_3 and D_3 increase in both viable and total volumes. Tumour A_3, which has q_1 and $V_d \approx 1$, experiences larger than average decreases and increases in viable and total volumes, respectively. By contrast, tumour C_3, which has an intermediate value of V_d, experiences larger than average increases in viable and total volumes (Colour figure online)

behaviour is observed for tumour B_3, with less RT-induced cell death and dead material accumulation as the oxygen concentration remains significantly lower than for A_3. As a result, the increase in total volume is also smaller. For tumour D_3, cell death due to RT and hypoxia is outweighed by the tumour regrowth between fractions, leading to small increases in viable and total volumes.

Further, while tumour C_3 lies closest to the SL region ($V_d \approx 0.8$), it does not transition from the basin of attraction of its NL steady state to its SL steady state, unlike tumours A_3 and B_3. In particular, the increase in the oxygen concentration for C_3 is not sufficiently rapid for the tumour to enter, during treatment, a SL regime where, on average, $c > c_{min}$. Therefore, the increase in viable volume is constant, but gradual, with a smaller accumulation of dead material. This explains why C_3 undergoes a larger than average increase in viable volume, with a moderate increase in total volume.

In summary, we have identified two extremal regions of parameter space in which tumours in a BS regime undergo larger decreases or increases in viable volume (and larger increases in total volume) than the typical tumour in this regime. Tumours which are sufficiently near to the boundary of the BS and SL regimes and consume little oxygen for maintenance experience larger than average decreases in viable cell volume as RT cell death is enhanced by higher oxygen levels. By contrast, tumours which are close to the boundary between the BS and SL regimes, but not sufficiently close, undergo larger than average increases in viable volume, regardless of the value
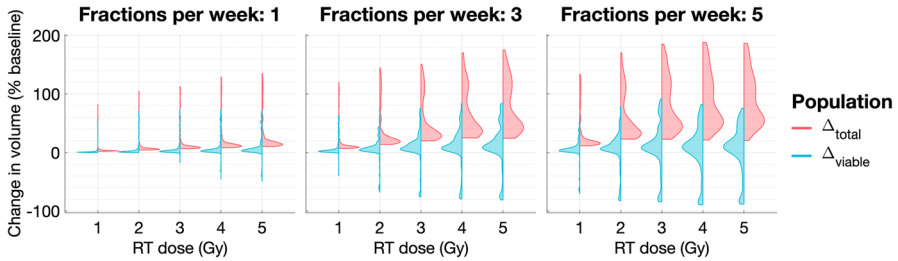
Fig. 16 For the virtual BS population, we show how the distributions of Δ_{viable} and Δ_{total} change as the dose rate, $R \in \{0.1, 0.2, 0.3, 0.4, 0.5\}$, and the number of fractions per week, $N_{frac} \in \{1, 3, 5\}$, vary. The mean and maximum values of Δ_{viable} increase, while its minimum value decreases, as R and N_{frac} increase. The mean, minimum and maximum values of Δ_{total} increase as R and N_{frac} increase. There is an exception for $N_{frac} = 5$, where the maximum value of Δ_{viable} and minimum value of Δ_{total} decrease with $R \geq 3$ (Colour figure online)

of q_1. This occurs as they attempt and fail to transition from their NL steady state to their SL steady state and, thus, RT cell death remains limited by low oxygen levels and outweighed by tumour regrowth between fractions.

The effect of the dosing schedule on typical tumour response. For the virtual population of tumours in a BS regime, we show in Fig. 16 how the dose rate, R, and the number of fractions per week, N_{frac}, affect tumour response to RT when the total dose is fixed. On average, a higher number of fractions per week (for fixed R) and a higher dose rate (for fixed N_{frac}) lead to greater increases in the viable and total cell populations. While these results contrast with those for tumours in SL regimes, we see that the maximum reduction in viable volume increases with R and N_{frac}, similarly to SL tumours. Overall, these results indicate that, in most cases, increasing the RT dose and frequency may be deleterious (similarly to NL tumours).

4.3 Post-treatment Tumour Growth Dynamics

In the previous section, we discussed the short-term response to RT of tumours in different growth regimes, distinguishing between tumours in monostable (NL and SL) and bistable regimes. We now investigate the long-term response to RT by studying post-treatment tumour growth dynamics and, in particular, the tumour steady states attained following treatment.

4.3.1 Steady State Analysis

We first perform a steady state analysis of the system (10)–(13) to understand the potential long-term effects of RT. Upon completion of a radiation protocol, we have $R \equiv 0$ thereafter. We, therefore, seek steady state solutions by setting $R = 0$ and $\frac{d}{dt} = 0$ in Eqs. (10)–(13) and solving the following system

$$q_2 c T(1 - \Sigma) - \delta_1(c_{min} - c)H(c_{min} - c)T + \mu T_S = 0, \tag{20}$$

$$\theta_2 q_2 c T_S(1 - \Sigma) - (\delta_{1,S}(c_{min} - c)H(c_{min} - c) + \mu + \xi)T_S = 0, \tag{21}$$

$$\xi T_S - \eta_R T_R = 0, \tag{22}$$

$$g(1-c)V_0 - q_1(T + \theta_1 T_S)c - q_3(T + \theta_2 T_S)c(1-\Sigma) = 0. \tag{23}$$

Denoting the steady state solutions by T^*, T_S^*, T_R^* and c^*, respectively, Eq. (22) implies that $T_S^* = \frac{\eta_R}{\xi} T_R^*$. Therefore, we have either $T_S^* = T_R^* = 0$ or $T_S^*, T_R^* > 0$. Suppose that $T_S^*, T_R^* > 0$. We can show, by contradiction, that there are no physically realistic steady state solutions satisfying this condition by, first, proving that there are no SL steady states with $T_S^*, T_R^* > 0$ and, then, proving that there are no NL steady states with $T_S^*, T_R^* > 0$.

If $c^* \geq c_{min}$, then Eq. (20) gives

$$T^* = \frac{-\mu T_S^*}{q_2 c^*(1-\Sigma^*)} < 0, \tag{24}$$

since $T_S^* > 0$ and $\Sigma^* < 1$ by assumption and $\mu > 0$ and $q_2 > 0$ by definition. Since $T^* > 0$ is required for a physically realistic solution, there are no SL steady states with $T_S^*, T_R^* > 0$.

If $0 < c^* < c_{min}$, then Eq. (20) implies that

$$\frac{q_2}{\delta_1}(1-\Sigma^*) - \frac{(c_{min} - c^*)}{c^*} = -\frac{\mu T_S^*}{\delta_1 c^* T^*} < 0. \tag{25}$$

Since $q_2 = \delta_1$, we have

$$(1-\Sigma^*) - \frac{(c_{min} - c^*)}{c^*} = -\frac{\mu T_S^*}{\delta_1 c^* T^*} < 0. \tag{26}$$

Then, Eq. (21) implies that

$$\frac{\theta_2 q_2}{\delta_{1,S}}(1-\Sigma^*) - \frac{(c_{min} - c^*)}{c^*} = \frac{(\mu + \xi)}{\delta_{1,S} c^*} > 0. \tag{27}$$

Since $\theta_2 q_2 = \delta_{1,S}$, we have

$$(1-\Sigma^*) - \frac{(c_{min} - c^*)}{c^*} = \frac{(\mu + \xi)}{\delta_{1,S} c^*} > 0. \tag{28}$$

Comparing Eqs. (26) and (28), we obtain a contradiction. This implies that there are no NL steady states with $T_S^*, T_R^* > 0$. We, therefore, conclude that NL and SL steady state solutions of the system (10)–(13) must have $T_S^* = T_R^* = 0$. It is then straightforward to show that the solutions of the system (20)–(23) with $T_S^* = T_R^* = 0$ are equal to the steady state solutions in the absence of treatment (Colson et al. 2022) (see Appendix A).

We have shown that RT preserves the steady states and growth regimes observed in the absence of treatment. We conclude that, given $T(0) = T^*$, tumours in monostable regimes at the start of treatment will return to their original tumour volume, $\Sigma_0 =$
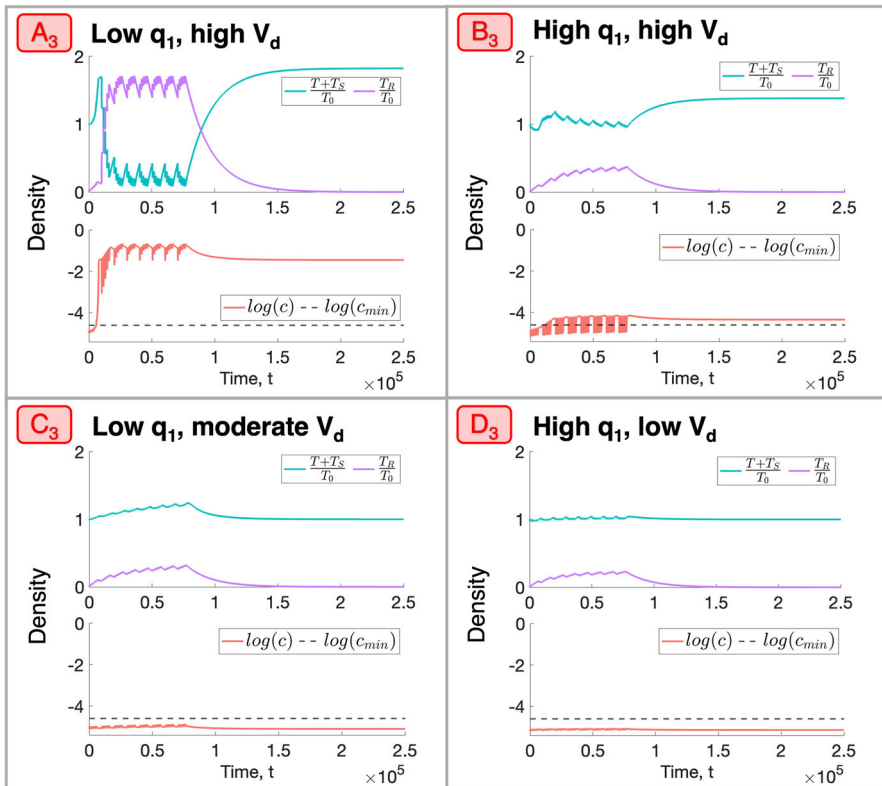
Fig. 17 For a conventional fractionation schedule, we numerically solve Eqs. (10)–(13) for $t \in (0, 2.5 \times 10^5]$ subject to the initial conditions (15). In A_3-D_3, we fix $V_0 = 0.00275$ and (q_1, q_3) as indicated by the points A_3, B_3, C_3 and D_3 in Fig. 14, which correspond to tumours in a BS regime. Tumours C_3 and D_3 evolve to their NL steady states following treatment, whereas tumours A_3 and B_3 switch to their SL steady states (Colour figure online)

$T^* + V_0$, and composition ($T_S^* = T_R^* = 0$) after RT. In contrast, tumours in a BS regime either return to the original, NL steady state, or evolve to the SL steady state.

4.3.2 Elucidating Conditions for RT to Drive Steady State Switching of Tumours in Bistable Regimes

The steady state analysis showed that tumours in a BS regime may attain either a NL or a SL steady state following treatment. In particular, such tumours may undergo large increases in tumour volume in response to RT as they switch from a NL steady state to a larger SL steady state. Recall the tumours A_3-D_3 that we defined in Sect. 4.2.2: Fig. 17 shows their response to RT both during, and following, a conventional fractionation schedule.

Tumours C_3 and D_3 underwent increases in viable volume during treatment and then returned to their NL steady states following treatment: the effect of RT was not strong enough to cause a switch in steady state. By contrast, tumours A_3 and B_3
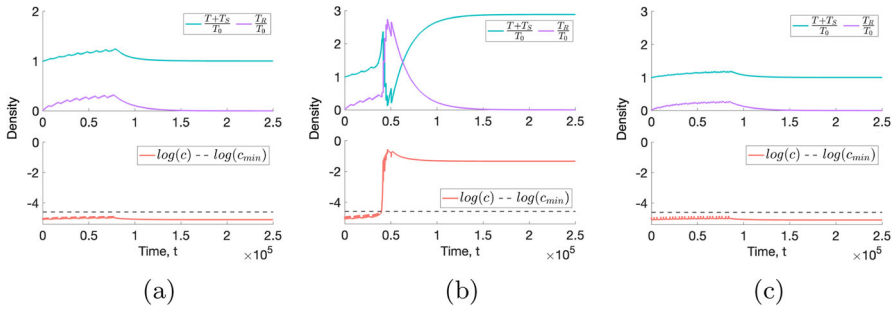
Fig. 18 We numerically solve Eqs. (10)–(13) for $t \in (0, 2.5 \times 10^5]$ subject to the initial conditions (15). We fix dose rates (**a**) $R = 0.2$ and (**b**), (**c**) $R = 0.3$ and simulate (**a**) daily fractions, Monday to Friday, for 8 weeks, (**b**) daily fractions, Monday to Friday, for 5.2 weeks and (**c**) fractions on Monday, Wednesday and Friday for 8.67 weeks. We fix $V_0 = 0.00275$ and (q_1, q_3) as indicated by parameter set C_3 in Table 4. Comparing (**a**), (**b**) and (**c**), we observe that lower RT doses and less frequent dosing both prevent the tumour C_3 from evolving to the SL steady state following treatment (Colour figure online)

experienced reductions in viable volume during treatment and then evolved to their SL steady states following treatment. The oxygen concentration in both of these tumours increased beyond the hypoxic threshold, c_{min}, during (A_3) or following (B_3) RT and remained above this threshold level thereafter. This enabled the viable cell population to grow unchecked until the SL equilibrium was reached.

In contrast to tumours C_3 and D_3, we recall that tumours A_3 and B_3 are characterised by $V_d \approx 1$, where V_d is defined in (18). They are also, respectively, characterised by high and low values of q_1, the oxygen consumption rate for maintenance. This suggests that tumours which are near to the boundary between the BS and SL regions in parameter space are most susceptible to undergoing a switch in steady state volume in response to RT, irrespective of the value of q_1. This observation holds across a range of RT protocols (see Appendix C).

We now consider how the dosing schedule affects the long-term dynamics of tumours in a BS regime. In Fig. 18a, b, we show the response of tumour C_3 to two fractionation protocols comprising either 2 or 3 Gy fractions applied 5 times per week for 8 or 5.2 weeks, respectively. A switch in steady state is observed for 3 Gy fractions. This suggests that the likelihood of a tumour switching steady state increases with dose, a consistent trend in our numerical study (see Appendix C). Figure 18c additionally shows the response of tumour C_3 to 3 Gy fractions applied 3 times per week for 8.67 weeks. Comparing this figure to Fig. 18b highlights how a lower dosing frequency can prevent the transition from a NL to a SL steady state for tumours in BS regimes (see Appendix C).

These results suggest that a lower RT dose and dosing frequency may prevent uncontrolled increases in tumour volume following RT for tumours in BS regimes. As with our observations for short-term treatment responses, this challenges the assumption that a higher dose, applied with a higher frequency, will lead to a greater reduction in tumour volume.

5 Discussion

Cancer is a heterogeneous disease. In particular, tumours can exhibit widely varying responses to treatments. As a result, the success of existing therapies, which are typically applied following a "one-size-fits-all approach", can be highly variable. Patient-specific treatment design could aid in overcoming these barriers to treatment efficacy, but this requires increased understanding of the factors which affect tumour sensitivity to treatment. In this paper, we investigated how two distinct mechanisms of growth arrest can influence tumour responses to radiotherapy (RT).

We extended an existing model of solid tumour growth which distinguishes between nutrient limited (NL) and space limited (SL) growth control (Colson et al. 2022). In the absence of treatment, this model exhibits three growth regimes: (i) NL, where a tumour attains a NL steady state at which cell proliferation and death balance, (ii) SL, where a tumour attains a SL steady state when cell proliferation ceases due to space constraints, with no cell death, and (iii) bistable (BS), where stable NL and SL steady states coexist. In this paper, we investigated how tumours in each regime respond to RT. We found that the short- and long-term responses of tumours in monostable regimes (i.e., NL and SL) can be distinguished from those of tumours in BS regimes.

Tumours in the SL regime typically respond well to RT in the short-term, as both their viable and total volumes decrease during fractionation, while tumours in the NL regime typically respond less well, since their total volume increases despite a reduction in viable volume. However, certain NL and SL tumours respond significantly better than the average tumour in their respective regimes. By identifying parameter regions which give rise to these outliers, we determined different mechanisms that underpin successful RT. For NL tumours, RT efficacy is maximised when regrowth between fractions is minimised, while, for SL tumours, increased RT efficacy may be due to limited regrowth (as for NL tumours) and/or RT cell kill. The additional SL-specific mechanism is a consequence of low rates of RT cell kill for NL tumours due to low oxygenation. This explains how the different growth arrest mechanisms that characterise the NL and SL regimes can affect short-term tumour response to RT. In the long-term, tumours in the NL and SL regimes always return to their pre-treatment steady state volume, irrespective of the effects of RT during treatment. Our model, therefore, predicts that any change in the tumour burden during radiation is transient for these tumours. This result follows from our simplifying assumption that the vascular volume remains constant during tumour growth and RT. We explain below how we could extend the model to relax this assumption.

We also found that most tumours in the BS regime respond badly to RT in the short-term, as their viable and total cell volumes increase during RT. As for monostable regimes, outliers which lie, in parameter space, near the boundary between BS and SL regions, exhibit more extreme responses to RT. In these cases, the intratumoural oxygen concentration is close to, and smaller than, c_{min}, the threshold concentration below which cells die due to nutrient insufficiency. If RT induces a net increase in oxygen levels such that $c > c_{min}$, then cell death due to nutrient insufficiency ceases and RT drives the tumour to its SL steady state. This leads to a significant increase in RT-induced cell death and dead cell accumulation, resulting in large decreases and increases in viable and total volumes, respectively. By contrast, if RT induces a

net increase in oxygen levels such that $c \leq c_{min}$, then RT causes large increases in viable and total volumes as the tumour grows towards, and fails to reach, its SL steady state. Here, RT cell kill is outweighed by tumour growth between fractions throughout treatment. Irrespective of whether these outliers experience increases or decreases in viable volume, they evolve to their larger SL steady state following RT. Therefore, the model predicts that, in the BS regime, RT usually has a detrimental effect on tumour growth.

A final key result relates to RT dosing schedules. We found that, in SL regimes, applying larger doses at higher frequency typically increases RT efficacy, whereas, in NL and BS regimes, administering lower doses at lower frequency can increase RT efficacy for outliers and lessen, or prevent, large increases in tumour burden across the virtual cohorts. The latter is a counter-intuitive result and challenges the assumption that giving the maximum tolerable dose is the best course of treatment. In practice, we are unlikely to know in which growth regime a patient's tumour lies when treatment starts. It would be interesting, in future work, to investigate whether we can determine a tumour's growth regime by monitoring its response to a given treatment protocol. If we can establish that a tumour is in a SL regime, then this would allow us to adapt the treatment protocol to maximise the reduction in tumour burden, e.g., by increasing the RT dose or dosing frequency. Alternatively, if a tumour is in a NL or BS regime, then it might be preferable to halt treatment early in order to prevent large increases in tumour burden.

While some of our findings support experimentally and clinically observed phenomena, others challenge some common assumptions. The significance of these results is limited by the fact that they remain to be tested against relevant clinical and/or experimental data. In future work, we will aim to calibrate and validate our model using a range of experimental data, with the caveat that it may be difficult to estimate all of the parameters from the data. For instance, *in vitro* assays involving 2D monolayers, where all tumour cells have abundant nutrient and proliferate until they reach confluence (Kapałczyńska et al. 2018), could be used to test our predictions for SL tumours. Further, *in vitro* assays involving 3D spheroids, which reach an equilibrium at which cell proliferation and cell death rates balance (Costa et al. 2016), could be used to test our predictions for NL tumours. Finally, if we can determine a tumour's growth regime from its initial response to RT, then, as mentioned above, we could also use *in vivo* tumour data from mice treated with RT to test model predictions across regimes.

In addition to testing our model against experimental data, in future work we aim also to relax some of its simplifying assumptions. First, we will view the vascular volume as a dynamic variable, which evolves in response to treatment and angiogenic signalling. In doing so, we will obtain a more realistic description, not only of the co-evolution of the tumour cells and vasculature, but also of responses to treatments which affect tumour and endothelial cells. In particular, if the vascular volume evolves over time, then treatment may alter the steady state tumour volumes. Second, since we found that the response of certain tumours (e.g., SL tumours) improves with higher doses applied at higher frequency, it would be interesting to incorporate a trade-off between anti-tumour effects and detrimental side-effects. For example, we could model the damage experienced by surrounding healthy tissue following each RT dose and impose a maximum value of cumulative damage over the RT protocol, above which

the RT toxicity is considered intolerable (e.g., see Hanin and Zaider 2013; Huang et al. 2015; Kuznetsov and Kolobov 2023; Stocks et al. 2017). This would enable us to assess which dosing regimens are clinically feasible and to evaluate tumour responses to RT protocols designed using the maximum tolerated dose.

Declarations

Conflicts of interest We declare we have no competing interests.

Code Availability MATLAB code to generate the three virtual tumour populations and to numerically solve the ODE model is available at: https://github.com/chloeacolson/InvestigatingTumourResponsesRadiotherapy.

Appendix A Steady State Solutions in the Absence of Treatment

A steady state analysis of the system (10)-(13) with $R \equiv 0$ was performed in Colson et al. (2022). There exist two SL steady states, given by

$$\text{SS}_1: \quad (T_1^*, c_1^*) = (0, 1), \tag{A1}$$

$$\text{SS}_2: \quad (T_2^*, c_2^*) = \left(1 - V_0, \frac{V_0}{V_0 + (q_1/g)(1 - V_0)}\right). \tag{A2}$$

SS_1 is unstable for all combinations of parameters, while SS_2 is stable in the parameter regions in which it is an admissible solution.

There are also two NL steady states, given by

$$\text{SS}_3: \quad (T_3^*, c_3^*) = (T(c_-), c_-) \tag{A3}$$

$$\text{SS}_4: \quad (T_4^*, c_4^*) = (T(c_+), c_+), \quad \text{if } V_0 \neq \frac{2(q_3 - q_1)}{g + q_3 - q_1}, \tag{A4}$$

where

$$T(c) = (1 - V_0) - \left(\frac{c_{min}}{c} - 1\right), \tag{A5}$$

and

$$
\begin{cases}
c_\pm = \frac{c_{min}(X \mp \sqrt{X^2 + 4q_3 Y})}{2Y}, & \text{if } V_0 \neq \frac{2(q_3 - q_1)}{g + q_3 - q_1}, \quad \text{(A6a)} \\
c_- = \frac{c_{min}(q_3(g + q_3 - q_1))}{2\frac{g}{c_{min}}(q_1 - q_3) - g(q_1 - 3q_3) + (q_1 - q_3)^2}, & \text{if } V_0 = \frac{2(q_3 - q_1)}{g + q_3 - q_1}, \quad \text{(A6b)}
\end{cases}
$$

with

$$
\begin{cases}
X = q_1 - 3q_3 + \left(\frac{g}{c_{min}} + q_3\right) V_0, \\
Y = 2(q_1 - q_3) + (g + q_3 - q_1) V_0.
\end{cases} \tag{A7}
$$

In the regions in which SS_3 and SS_4 exist as admissible steady state solutions, SS_3 is stable, while SS_4 is unstable.

Appendix B Sampling the (q_1, q_3) Pairs that Define the NL, SL and BS Virtual Tumour Populations

From Fig. 2, it is straightforward to see that, for fixed V_0, there exists a threshold value of q_1, say $\bar{q}_1$, such that the parameter set (q_1, q_3, V_0) corresponds to a tumour which lies in the NL regime for all $q_1 \geq \bar{q}_1$ and $q_3 > 0$. We also see that, for fixed V_0 and $q_1 < \bar{q}_1$, there exists a threshold value of q_3, say $\bar{q}_3$, such that the parameter set (q_1, q_3, V_0) corresponds to a tumour which lies in the SL regime for all $q_3 < \bar{q}_3$ and in the BS regime for all $q_3 \geq \bar{q}_3$.

Using the stable NL and SL steady state solutions in the absence of treatment defined in Eqs. (A2) and (A3), we derive the following analytical expressions for $\bar{q}_1$ and $\bar{q}_3$

$$
\bar{q}_1 = g\left(\frac{1}{c_{min}} - 1\right)\frac{V_0}{1 - V_0}, \tag{B8}
$$

$$
\bar{q}_3 = \frac{-q_1 + \left(\frac{3g}{c_{min}} - 2 + q_1\right) V_0 - \frac{g}{c_{min}} V_0^2}{(1 - V_0)^2} + \frac{2g^{1/2}}{(1 - V_0)^2} \times
$$
$$
\left[-\left(\frac{2}{c_{min}} - 1\right) q_1 V_0 + \left(g\left(\frac{2}{c_{min}^2} - \frac{3}{c_{min}} + 1\right) + q_1\left(\frac{3}{c_{min}} - 1\right)\right) V_0^2 \right.
$$
$$
\left. - \left(g\left(\frac{1}{c_{min}^2} - \frac{1}{c_{min}}\right) + \frac{q_1}{c_{min}}\right) V_0^3 \right]^{1/2}. \tag{B9}
$$

We note that, for fixed $c_{min} = 0.01$ and $g = 5$, $\bar{q}_1$ depends only on V_0, while $\bar{q}_3$ depends on V_0 and q_1.

Using (B8) and (B9), we define the uniform distributions $U(a, b)$ used to sample the pairs of q_1 and q_3 values that correspond to the NL, SL and BS cohorts, respectively, in Table 5. The code used to generate the (q_1, q_3) pairs for each cohort and the parameter

Table 5 Uniform distributions $U(a, b)$ used to sample the pairs of q_1 and q_3 values that correspond to the NL, SL and BS cohorts, respectively. $\bar{q}_1$ and $\bar{q}_3$ are defined by Eqs. (B8) and (B9), respectively

Cohort	NL	SL	BS
Distribution used to sample q_1	$U(\bar{q}_1, 10)$	$U(0.01, \bar{q}_1)$	$U(0.01, \bar{q}_1)$
Distribution used to sample q_3	$U(0.01, 10)$	$U(0.01, \bar{q}_3)$	$U(\bar{q}_3, 10)$

sets which define the three cohorts considered in this paper are available at: https://github.com/chloeacolson/InvestigatingTumourResponsesRadiotherapy.

Appendix C Numerical Results: Steady State Switching of Tumours in the Bistable Regime

For dosing regimens with $R \in \{0.1, 0.3, 0.5\}$ and $N_{frac} \in \{1, 3, 5\}$, the scatter plots in Fig. 19 highlight (in red) the (q_1, V_d) pairs which correspond to tumours in a bistable regime that switch steady state. We observe that tumours which switch steady state typically have larger values of V_d. We note also that the number of tumours which switch steady state increases with R and N_{frac}. These results are consistent with those presented in Sect. 4.3.2 for tumour C_3.
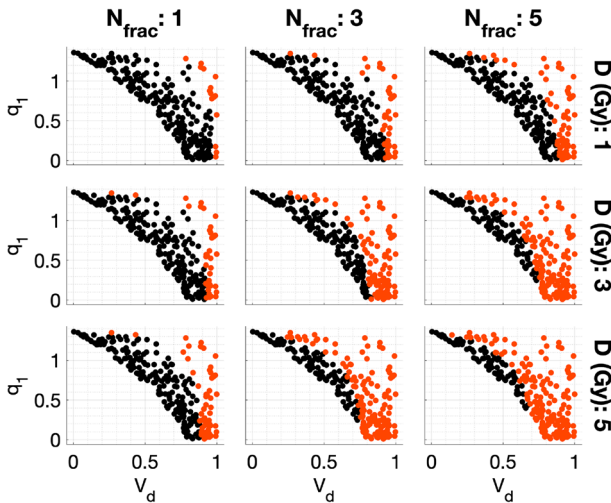

Fig. 19 For the virtual BS tumour population and fractionation schedules with $R \in \{0.1, 0.3, 0.5\}$ and $N_{frac} \in \{1, 3, 5\}$, the scatter plots show the (q_1, V_d) pairs that correspond to tumours that switch (red) and do not switch (black) steady state. The former are typically characterised by larger values of V_d (Colour figure online)

References

Ahmed KA, Correa CR, Dilling TJ et al (2014) Altered fractionation schedules in radiation treatment: a review. Semin Oncol 41(6):730–750. https://doi.org/10.1053/j.seminoncol.2014.09.012

Alfonso J, Berk L (2019) Modeling the effect of intratumoral heterogeneity of radiosensitivity on tumor response over the course of fractionated radiation therapy. Radiat Oncol 14(1):1–12. https://doi.org/10.1186/s13014-019-1288-y

Alfonso J, Jagiella N, Núnez L et al (2014) Estimating dose painting 506 effects in radiotherapy: a mathematical model. PloS One 9(2):e89380. https://doi.org/10.1371/journal.pone.0089380

Belfatto A, Jereczek-Fossa BA, Baroni G et al (2018) Model-supported radiotherapy personalization: in silico test of hyper-and hypo-fractionation effects. Front Physiol 9:1445. https://doi.org/10.3389/fphys.2018.01445

Bernard S, Herzel H (2006) Why do cells cycle with a 24 hour period? Genome Inform 17(1):72–79

Celora GL, Byrne HM, Kevrekidis P (2023) Spatio-temporal modelling of phenotypic heterogeneity in tumour tissues and its impact on radiotherapy treatment. J Theor Biol 556(111):248. https://doi.org/10.1016/j.jtbi.2022.111248

Colson C, Byrne HM, Maini PK (2022) Combining mechanisms of growth arrest in solid tumours: a mathematical investigation. Bull Math Biol 84(8):1–24. https://doi.org/10.1007/s11538-022-01034-2

Costa EC, Moreira AF, de Melo-Diogo D et al (2016) 3d tumor spheroids: an overview on the tools and techniques used for their analysis. Biotechnol Adv 34(8):1427–1441

Curtis SB (1986) Lethal and potentially lethal lesions induced by radiation—a unified repair model. Radiat Res 106(2):252–270. https://doi.org/10.2307/3576798

Dormand JR, Prince PJ (1980) A family of embedded Runge-Kutta formulae. J Comput Appl Math 6(1):19–26. https://doi.org/10.1016/0771-050X(80)90013-3

Drasdo D, Höhme S (2005) A single-cell-based model of tumor growth in vitro: monolayers and spheroids. Phys Biol 2(3):133. https://doi.org/10.1088/1478-3975/2/3/001

Enderling H, Anderson AR, Chaplain MA et al (2006) Mathematical modelling of radiotherapy strategies for early breast cancer. J Theor Biol 241(1):158–171. https://doi.org/10.1016/j.jtbi.2005.11.015

Enderling H, Park D, Hlatky L et al (2009) The importance of spatial distribution of stemness and proliferation state in determining tumor radioresponse. Math Model Nat Phenom 4(3):117–133. https://doi.org/10.1051/mmnp/20094305

Enderling H, Chaplain MA, Hahnfeldt P (2010) Quantitative modeling of tumor dynamics and radiotherapy. Acta Biotheor 58(4):341–353. https://doi.org/10.1007/s10441-010-9111-z

Gad S (2014) Maximum tolerated dose. In: Wexler P (ed) Encyclopedia of toxicology, 3rd edn. Academic Press, Oxford, p 164. https://doi.org/10.1016/B978-0-12-386454-3.00874-5

Goodhead DT (1985) Saturable repair models of radiation action in mammalian cells. Radiat Res 104(2s):S58–S67. https://doi.org/10.2307/3583513

Graham K, Unger E (2018) Overcoming tumor hypoxia as a barrier to radiotherapy, chemotherapy and immunotherapy in cancer treatment. Int J Nanomed 13:6049. https://doi.org/10.2147/IJN.S140462

Greenspan HP (1972) Models for the growth of a solid tumor by diffusion. Stud Appl Math 51(4):317–340. https://doi.org/10.1002/sapm1972514317

Hahnfeldt P, Panigrahy D, Folkman J et al (1999) Tumor development under angiogenic signaling: a dynamical theory of tumor growth, treatment response, and postvascular dormancy. Can Res 59(19):4770–4775

Hanin L, Zaider M (2013) A mechanistic description of radiation-induced damage to normal tissue and its healing kinetics. Phys Med Biol 58(4):825

Hillen T, Enderling H, Hahnfeldt P (2013) The tumor growth paradox and immune system-mediated selection for cancer stem cells. Bull Math Biol 75(1):161–184. https://doi.org/10.1007/s11538-012-9798-x

Huang BT, Lu JY, Lin PX et al (2015) Radiobiological modeling analysis of the optimal fraction scheme in patients with peripheral non-small cell lung cancer undergoing stereotactic body radiotherapy. Sci Rep 5(1):1–9

Jeong J, Oh JH, Sonke JJ et al (2017) Modeling the cellular response of lung cancer to radiation therapy for a broad range of fractionation schedules. Clin Cancer Res 23(18):5469–5479. https://doi.org/10.1158/1078-0432.CCR-16-3277

Kapałczyńska M, Kolenda T, Przybyła W et al (2018) 2d and 3d cell cultures-a comparison of different types of cancer cell cultures. Arch Med Sci 14(4):910–919

Konopacka M, Rogoliński J, Sochanik A et al (2016) Can high dose rates used in cancer radiotherapy change therapeutic effectiveness? Contempor Oncol/Współczesna Onkologia 20(6):449–452. https://doi.org/10.5114/wo.2016.65603

Kuznetsov M, Kolobov A (2023) Optimization of antitumor radiotherapy fractionation via mathematical modeling with account of 4 R's of radiobiology. J Theor Biol 558(111):371

Lewin TD, Maini PK, Moros EG et al (2018) The evolution of tumour composition during fractionated radiotherapy: implications for outcome. Bull Math Biol 80(5):1207–1235. https://doi.org/10.1007/s11538-018-0391-9

Lewin TD, Maini PK, Moros EG et al (2020) A three phase model to investigate the effects of dead material on the growth of avascular tumours. Math Model Nat Phenom 15:22. https://doi.org/10.1051/mmnp/2019039

Liu J, Hormuth DA, Davis T et al (2021) A time-resolved experimental-mathematical model for predicting the response of glioma cells to single-dose radiation therapy. Integr Biol. https://doi.org/10.1093/intbio/zyab010

Maier P, Hartmann L, Wenz F et al (2016) Cellular pathways in response to ionizing radiation and their targetability for tumor radiosensitization. Int J Mol Sci 17(1):102. https://doi.org/10.3390/ijms17010102

Marques FG, Carvalho L, Sousa JS et al (2020) Low doses of ionizing radiation enhance angiogenesis and consequently accelerate post-embryonic development but not regeneration in zebrafish. Sci Rep 10(1):1–8. https://doi.org/10.1038/s41598-020-60129-9

McMahon SJ (2018) The linear quadratic model: usage, interpretation and challenges. Phys Med Biol 64(1):01TR01. https://doi.org/10.1088/1361-6560/aaf26a

Milzman J, Sheng W, Levy D (2021) Modeling lsd1-mediated tumor stagnation. Bull Math Biol 83(2):1–29

National Cancer Institute (2019) Radiation therapy. https://www.cancer.gov/about-cancer/treatment/types/radiation-therapy. Accessed 2 Oct 2022

National Cancer Institute (2022) Chemotherapy. https://www.cancer.gov/about-cancer/treatment/types/chemotherapy. Accessed 2 Oct 2022

Neira S, Gago-Arias A, Guiu-Souto J et al (2020) A kinetic model of continuous radiation damage to populations of cells: comparison to the LQ model and application to molecular radiotherapy. Phys Med Biol 65(24):245015. https://doi.org/10.1088/1361-6560/aba21d

Powathil G, Kohandel M, Milosevic M et al (2012) Modeling the spatial distribution of chronic tumor hypoxia: implications for experimental and clinical studies. Comput Math Methods Med. https://doi.org/10.1155/2012/410602

Prokopiou S, Moros EG, Poleszczuk J et al (2015) A proliferation saturation index to predict radiation response and personalize radiotherapy fractionation. Radiat Oncol 10(1):1–8

Rockne R, Alvord E, Rockhill J et al (2009) A mathematical model for brain tumor response to radiation therapy. J Math Biol 58(4):561–578. https://doi.org/10.1007/s00285-008-0219-6

Steel GG, Deacon JM, Duchesne GM et al (1987) The dose-rate effect in human tumour cells. Radiother Oncol 9(4):299–310. https://doi.org/10.1016/s0167-8140(87)80151-2

Stocks T, Hillen T, Gong J et al (2017) A stochastic model for the normal tissue complication probability (NTCP) and applications. Math Med Biol J IMA 34(4):469–492

Stolz BJ, Kaeppler J, Markelc B et al (2022) Multiscale topology characterizes dynamic tumor vascular networks. Sci Adv 8(23):eabm2456. https://doi.org/10.1126/sciadv.abm2456

Tobias CA (1985) The repair-misrepair model in radiobiology: comparison to other models. Radiat Res 104(2s):S77–S95. https://doi.org/10.2307/3576635

Venkatesulu BP, Mahadevan LS, Aliru ML et al (2018) Radiation-induced endothelial vascular injury: a review of possible mechanisms. JACC Basic Transl Sci 3(4):563–572. https://doi.org/10.1016/j.jacbts.2018.01.014

Watanabe Y, Dahlman EL, Leder KZ et al (2016) A mathematical model of tumor growth and its response to single irradiation. Theor Biol Med Model 13(1):1–20. https://doi.org/10.1186/s12976-016-0032-7

Zahid MU, Mohamed AS, Caudell JJ et al (2021) Dynamics-adapted radiotherapy dose (dard) for head and neck cancer radiotherapy dose personalization. J Personal Med 11(11):1124. https://doi.org/10.3390/jpm11111124